AN ABSTRACT OF THE THESIS OF

Pierre Doguin for the degree of Master of Science in Geophysics presented on June 9, 1989

Title: Crustal Structure and Faulting of the Northern Gulf of California from Geophysical Modeling and Deconvolution of Magnetic Profiles.

Abstract approved: Redacted for Privacy

Using gravity, magnetic, bathymetric and seismic refraction data, I have constructed a geophysical cross-section of the central part of the northern Gulf of California. The section exhibits a crustal thickness of 18 km and features an anomalous block of high density lower basement (3.15 g/cm^3) which probably resulted from rifting processes during the opening of the Gulf. The magnetization of the upper basement ranges from 0.0005 to 0.0030 emu/cm^3. Three different layers of sediments are modeled, ranging from unconsolidated (1.85 g/cm^3) to compacted (2.50 g/cm^3).

I present a deconvolution method for automated interpretation of magnetic profiles based on Werner's (1953) simplified thin-dike assumption, leading to the linearization of complex nonlinear magnetic problems. The method is expanded by the fact that the horizontal gradient of the total

field caused by the edge of a thick interface body is equivalent to the total field of a thin dike. Statistical decision making and a seven point operator are used to insure good approximations of susceptibility, dip, depth, and horizontal location of the source. After using synthetic models to test the inversion method, I applied it to the Northern Gulf of California using data collected in 1984 by the Continental Margins Study Group at Oregon State University. Fault traces, computed by the deconvolution, are plotted on a map. The faulting pattern obtained is in good agreement with that proposed by other workers using other methods. The depths to the top of the faults range from 4 to 5 km in the eastern part of the Gulf, where they may be interpreted as the top of the structural basement. Deeper estimates are obtained for the western part of the Gulf.

Crustal Structure and Faulting of the Gulf of California fron Geophysical Modeling and Deconvolution of Magnetic Profiles

by

Pierre Doguin

A THESIS
submitted to
Oregon State University

in partial fulfillment of
the requirements for the
degree of

Master of Science

Completed on June 9, 1989
Commencement June 1990

APPROVED:

Redacted for Privacy

Associate Professor of Geophysics in charge of major

Redacted for Privacy

Dean of College of Oceanography

Redacted for Privacy

Dean of Graduate School

Date thesis is presented June 9, 1989

Typed by the author Pierre Doguin

ACKNOWLEDGMENTS

I would like to express my deepest thanks to my major professor, Dick Couch, for introducing me to marine geophysics when I was inexperienced in this field. His encouragement, advice, and timely travel hints were always appreciated.

My gratitude is extended to all the staff in CONMAR, for showing me the practical side of geophysics. The time spent there and aboard the Altair helped me solve that primordial question: donde chingados estamos?

My thanks to all the geophysics faculty members, especially to John Nabelek for jumping late on my committee wagon, and to Shaul Levi for his never ending good humor and spirit.

I enjoyed the times spent with my fellow students, Rainer who taught me that beer is not beer unless brewed under the German law, Haraldur for endlessly trying to have me pronounce his name correctly, and all the great guys from Mexico, Germany, Brazil, Pakistan and China, not to mention Iceland. Having the world come to you is surely one of the best ways to travel.

Five years spent studying, partying and travelling together in France and in the States sealed forever my friendship with geophysicists Michel and Yannick, and also with Alain and Pascal. Keeping the french spirit alive here at

OSU was a great asset to us, and will likely go on when I finally join them back in France.

Last but not least, my brothers and sister, and especially my parents deserve special thanks for their love and support during all these years away from home. This thesis is dedicated to all of them.

This work was supported by the Office of Naval Research under grant n° N00014-84-C-0673, and by the NASA Crustal Dynamics Project under grant n° NAG 5-788.

TABLE OF CONTENTS

LIST OF APPENDIX FIGURES

LIST OF FIGURES

LIST OF TABLES

CRUSTAL STRUCTURE AND FAULTING OF THE NORTHERN GULF OF CALIFORNIA FROM GEOPHYSICAL MODELING AND DECONVOLUTION OF MAGNETIC PROFILES

INTRODUCTION

The Gulf of California is part of the boundary between the North American and the Pacific tectonic plates. Faulting occurs throughout the length of the Gulf. It is mostly characterized by a series of "en échelon" transform faults connected by short spreading centers (Vine, 1966; Moore et al, 1968). Basins of the southern area are largely of oceanic type, while perhaps a transition between oceanic and continental crust characterizes the northern Gulf (Figure 1) where faults have more a strike-slip motion (Wilson, 1965), connecting with the San-Andreas fault system further north. Much of the northern Gulf is filled with a very thick layer of unconsolidated and semi-consolidated sediments, making it difficult to define the underlying basement structures. A better understanding of the tectonics of this area can be obtained through constructing geophysical cross-sections across the Gulf, such as the ones completed by Plawman (1978) north of the Gulf and by Calderon (1978) in the vicinity of Tiburon Island. In plan view, it is also possible to recover the structural information contained in the

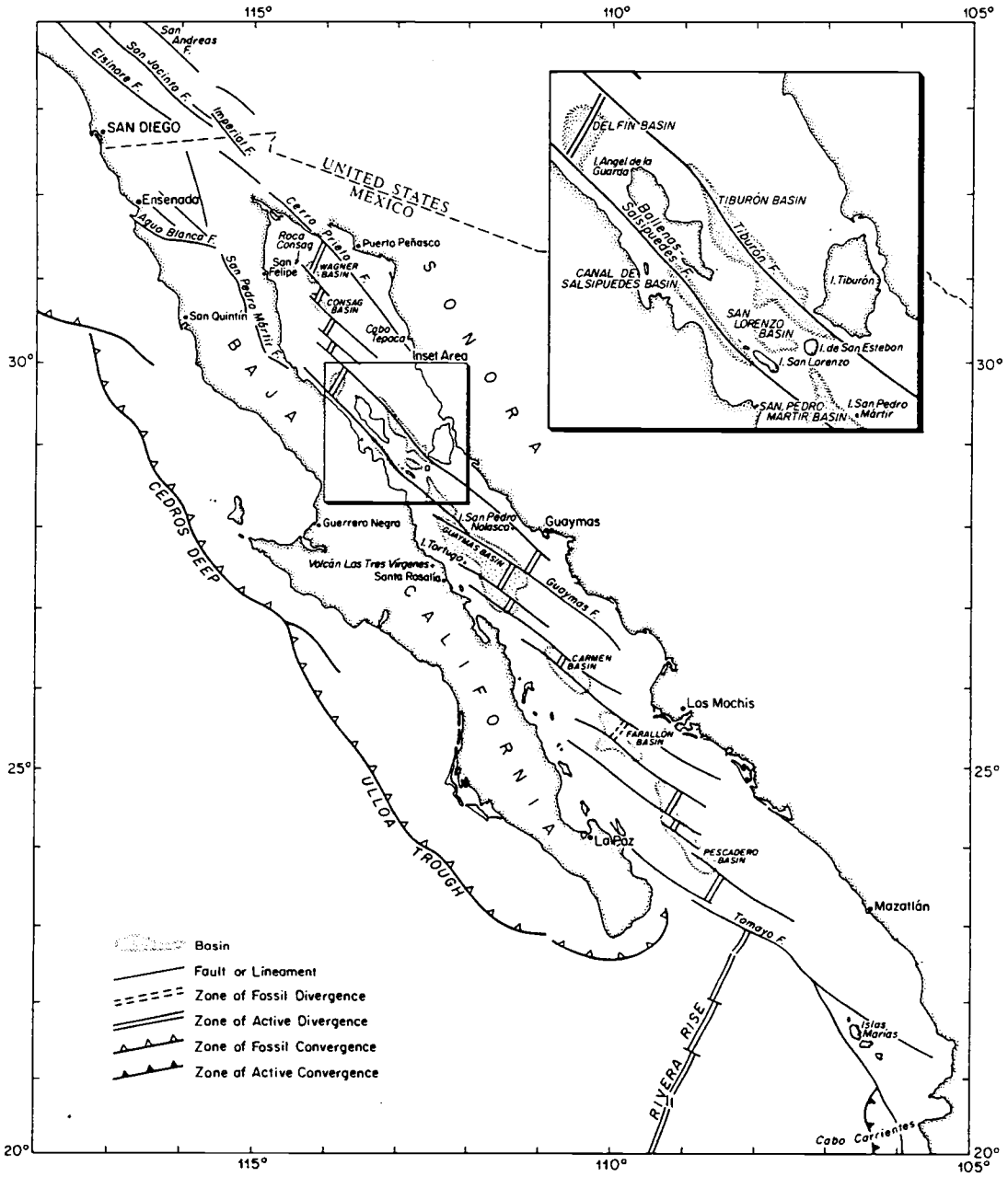

Figure 1. Tectonic map of the northern Gulf of California after Ness et al. (1988)

magnetic field anomalies via an automated method which locates fault positions along survey tracklines.

A joint program between the Geophysics Group at Oregon State University and the Mexican Direccion General de Oceanografica Naval (DGON) realized six geophysical cruises within the Pacific Exclusive Economic Zone of Mexico, including the Gulf of California. I use data from two of these cruises, GOLFO81 and GOLFO84, to construct a cross-section through the center of the northern Gulf, using precisely-navigated bathymetry, gravity and magnetic data, as well as published seismic refraction information. Magnetic data are also analyzed by deconvolution, based on the work of Werner (1953), to determine the location of faults, as well as their depth, dip angle and the susceptibility contrast of the surrounding materials.

PREVIOUS WORK

Numerous studies have been done in the northern Gulf of California in the past, as people realized the complexity of this area, but especially after the advancement of the sea-floor spreading concept (Vine, 1966). I will attempt here to summarize the ones that relate to my study.

An important early contribution to the understanding of the complex phenomena taking place within the northern Gulf of California was the work done by Rusnak et al. (1964). They compiled a bathymetric map, which was later used as the basis for a large number of subsequent studies, which identified the major basins and fault scarps of the Gulf. Based upon the strike-slip displacement figure of Crowell (1962), they suggested that the peninsula of Baja California had drifted away from mainland Mexico by as much as 260 km.

Phillips (1964) published the results of a marine seismic refraction survey conducted in 1959. Constraints from 12 stations in the northern Gulf of California allowed him to construct a series of crustal cross-sections. In particular, the section derived for the shallow area of the northern Gulf of California included 4 layers comprising 1.5 km of unconsolidated sediments and 4.3 km of basement material on top of the main crustal layer.

The first gravity survey in the northern Gulf of California was conducted by Harrison and Mathur (1964). Though the spacing of their tracklines north of 29°N was wider than between 27° N and 29° N, they constructed simple and complete Bouguer gravity anomaly maps, which suggested the presence of faults along the edges of the northernmost part of the Gulf.

Hilde (1964) directed the first magnetic survey in 1959, but only in the southern part of the Gulf. His study, conducted prior to the advent of plate tectonics, could not recognize the magnetic anomalies as manifestations of spreading centers.

One of the most reasonable models to date for the origin of the Gulf of California was done by Wilson (1965) when he discussed the fault system in the Gulf within the framework of his concept of transform faults. In his interpretation, the Gulf opened through a single ridge-to-ridge transform fault, the San Andreas, that connected the East Pacific Rise at the mouth of the Gulf of California with the Gorda Ridge off northern California.

Vine (1966) used this idea along with the concept of seafloor spreading and conceived the opening of the Gulf as being caused by spreading on the East Pacific Rise as it enters the southern Gulf of California and passes through it as a series of short spreading segments connected by transform faults, thus forming the en echelon morphological pattern first noted by Rusnak et al. (1964).

Sykes (1968) and Lomnitz et al. (1970) in studies of the distribution and focal mechanisms of earthquakes, lent detail to the locations of transform faults and spreading centers in the northern Gulf of California, and beneath the Colorado River delta and Imperial Valley, by relating earthquake activity to physiographic features.

Thatcher and Brune (1971) gave an account of the seismicity of the northern Gulf of California since 1962 and analyzed the occurrence of an earthquake swarm in the northern Gulf of California in the area of Wagner Basin. Their study provided important information on the structure and seismicity beneath two proposed spreading centers located in the Delfin and Wagner Basins. Seismic activity associated with the spreading centers of the northern Gulf occurs mainly in swarm-like events. The particular earthquake swarm they analyzed showed predominant normal fault mechanisms, and an upper crustal hypocentral depth.

Moore (1973) also used earthquake swarms to determine the position of spreading centers in the northern Gulf of California. He proposed a spreading center in the Delfin Basin, with a transform fault located between Angel de la Guarda Island and peninsular Baja California. This study also elaborated on the concept of the existence of a proto-gulf that existed between 4 and 10 million years ago.

The existence and location of faults and spreading centers in the Delfin and Wagner basins was also the result of the interpretation of seismic reflection profiles by Henyey and Bishoff

(1973). The profiles revealed a pattern similar to that caused by normal faulting and a high heat flow pattern in these basins. Their observations were consistent with the fault plane solutions of Thatcher and Brune (1971).

Klitgord et al. (1974) analyzed a series of magnetic profiles in order to detect anomalies created by sea-floor spreading. Though they failed to observe such patterns, they nevertheless concluded that while not proving the existence of spreading centers, it was consistent with it.

Plawman (1977), using gravity, magnetic and seismic refraction constraints, constructed two geophysical cross-sections north of the head of the Gulf of California in the Imperial Valley. He modeled depths to the Mohorovicic discontinuity of 20 km below the Imperial Valley and 22 km below the Colorado River delta.

Calderon Riveroll (1978) constructed two geophysical cross-sections in the central Gulf of California. Both sections were perpendicular to the main strike of the Gulf, and passed through Angel de la Guarda Island. Depth to the Moho was 12 km west of the island to 13 km east of it, and deepened toward the east, eventually becoming a continental type crust.

Fuis et al. (1984) conducted a seismic refraction survey of the Imperial Valley region in southern California. They modeled five seismic refraction profiles and built a gravity profile across the

Salton Trough. The profile revealed the presence of an anomalously low-density block of mantle material under the center of the trough.

Kasser et al. (1987) set up a trilateration network using laser telemetry in 1982 and 1986 across the central part of the Gulf . The deformation pattern during that period indicated a right lateral shear movement in the Gulf axis direction N46°W and a relative plate velocity of 8 cm/y.

Goff et al. (1987) analyzed data from major earthquakes to show mostly right-lateral strike-slip faulting along the transform faults of the Gulf, and two normal-faulting earthquakes in the northern Gulf displayed centroid depth of 6 km, consistent with that of other settings where a rifting process exists.

Sanchez-Zamora (1988) used spectral analysis of magnetic anomalies to obtain at least three distinct magnetic source horizons in the northern Gulf of California. He computed the depth to the bottom of the magnetized crust, interpreted as the Curie-point isotherm, to be an average of 11.5 km below sea level.

DATA ACQUISITION AND REDUCTION

Marine Surveys

I have used data from two geophysical surveys north of 27°N in the Gulf , both of which acquired bathymetric, gravity and magnetics data .

The first cruise (GOLFO-81) was conducted in the spring of 1981 using TRANSIT satellite positions and dead reckoning as the principal means of navigation. Fixes were received nominally every 90 minutes, and dead reckoning from gyro information was used between fixes. The navigation data were later adjusted to minimize differences in gravity values at course changes caused by the Eötvös acceleration which is very sensitive to navigation.

The other cruise, GOLFO-84, was conducted in the spring of 1984 using ARGO, a more precise navigation system. The ARGO system is a 21.8 MHz, pseudo-range-range transponder system, with a mobile unit on board the ship and three fixed transponders based on shore. The positions of the shore base-stations were determined using Magnavox 1502 Satellite Navigators. ARGO is a phase comparison, lane counting system that yields an uncertainty of about 5 meters in individual fixes. Land gravity data were also collected during this survey.

The combined tracklines obtained by the two cruises are shown in Figure 2. The tracklines were oriented such that they were perpendicular to the principal known and assumed structures of the Gulf. The distance between adjacent tracklines is of the order of 10 km.

Gravity Data

Marine gravity measurements were collected using Lacoste and Romberg Surface Ship Gravity Meter S-42, which was tied to the International Gravity Base Stations at San Diego and Guaymas using Lacoste and Romberg land meters. Digital data were recorded every 30 seconds during GOLFO-81, while the 1984 cruise sampled every 10 seconds. Both data sets were subsequently splined to remove offsets and then trimmed. The meter also corrected for cross-coupling effects by cross-correlation in real time.

Eötvös corrections were computed from navigation files and applied to the gravity data during post-processing. By subtracting the theoretical gravity values given by the International Gravity Field of 1967 from the observed gravity values, the free-air anomalies obtained showed a RMS trackline crossing discrepancy of 4.4 mGal for the 1981 cruise and 1.5 mGal for the 1984 survey.

Figure 3 shows the hand-contoured gravity anomaly map derived from these data.

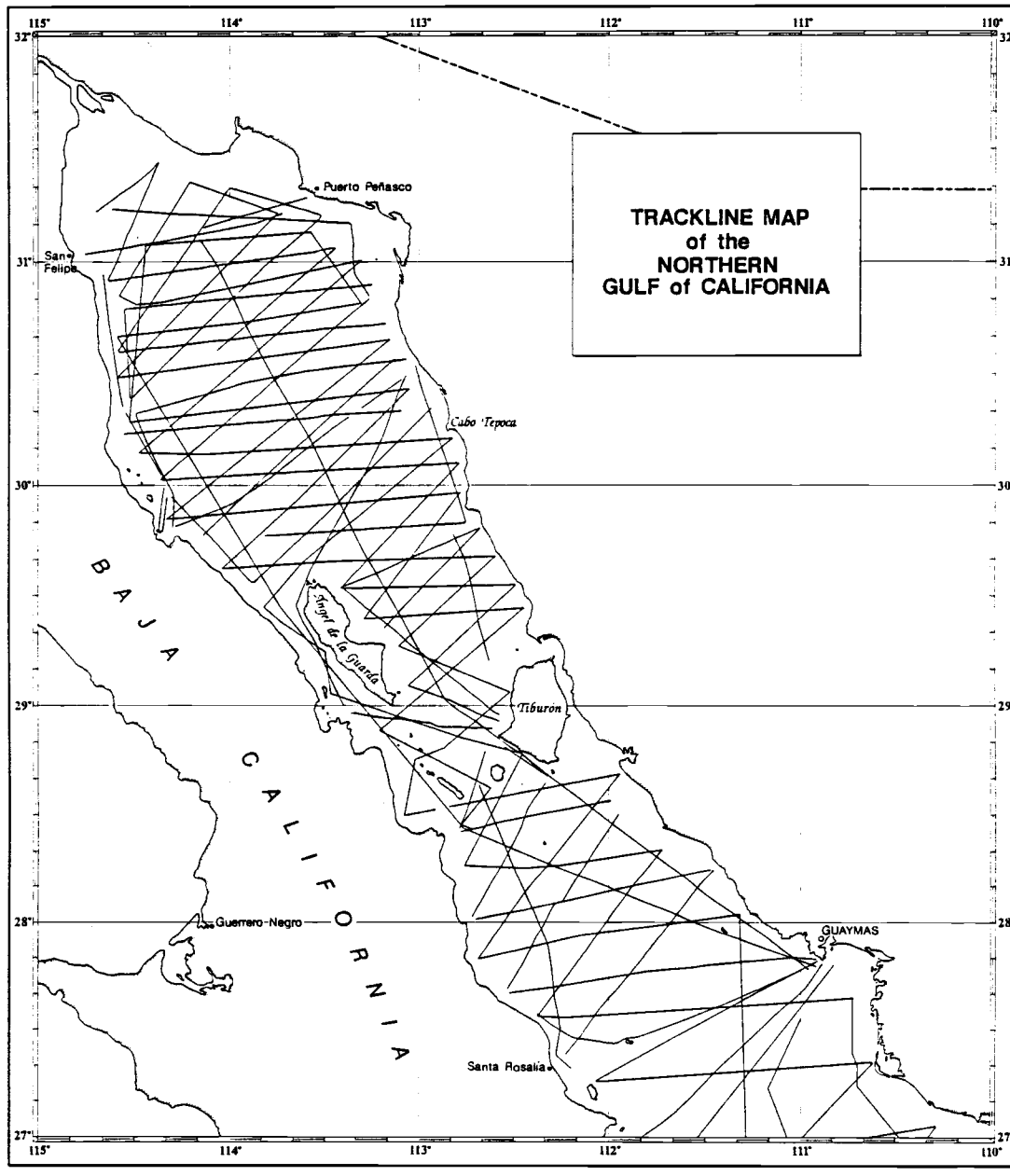

Figure 2. Gravity and magnetics trackline map.

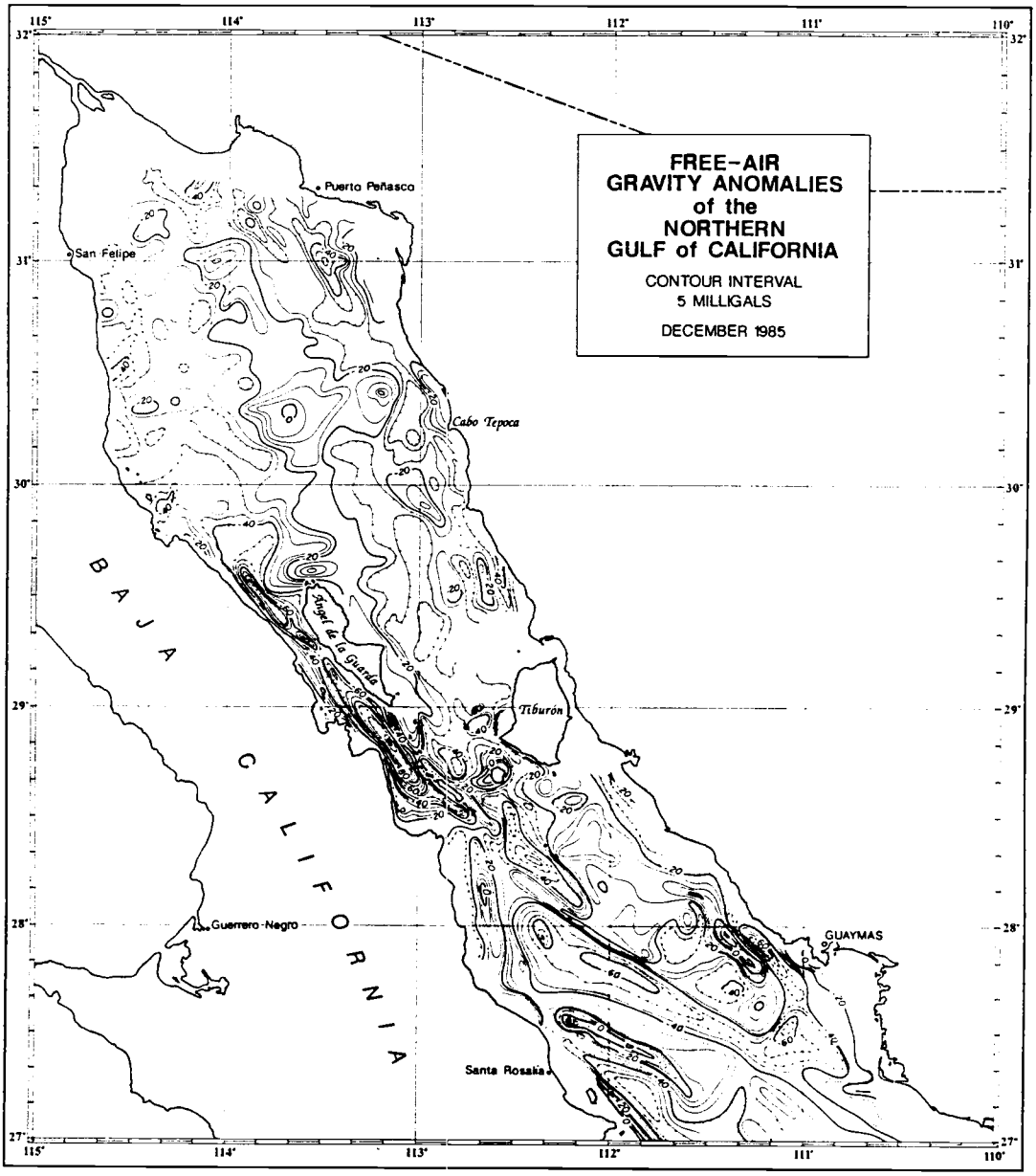

Figure 3. Free-air gravity anomaly map of the northern Gulf of California

Magnetics Data

The total magnetic field was measured using a Geometrics G-803 Marine/Airborne Proton Precession Magnetometer. The magnetics data were recorded every 30 seconds on the 1981 cruise and every 10 seconds on the 1984 survey. They, too, were later splined and trimmed. The total magnetic field anomaly was calculated by taking the difference between the International Geomagnetic Reference Field of 1980 and the observed total field values, yielding a RMS trackline crossing discrepancy of 17.2 nT for the 1984 cruise. No RMS discrepancy was computed for the 1981 cruise.

The hand-contoured total field anomaly map is shown on Figure 4.

Gridding

Since the location of the geophysical cross-section described later was selected primarily for its proximity to seismic refraction data, the section does not coincide with a particular trackline. Furthermore, the method used for the Werner deconvolution requires a regularly spaced data set. Three grids were therefore constructed from bathymetric, gravity and magnetics data, using the minimum curvature algorithm of Briggs (1974), which minimizes the curvature of a surface through the value at each point. The three

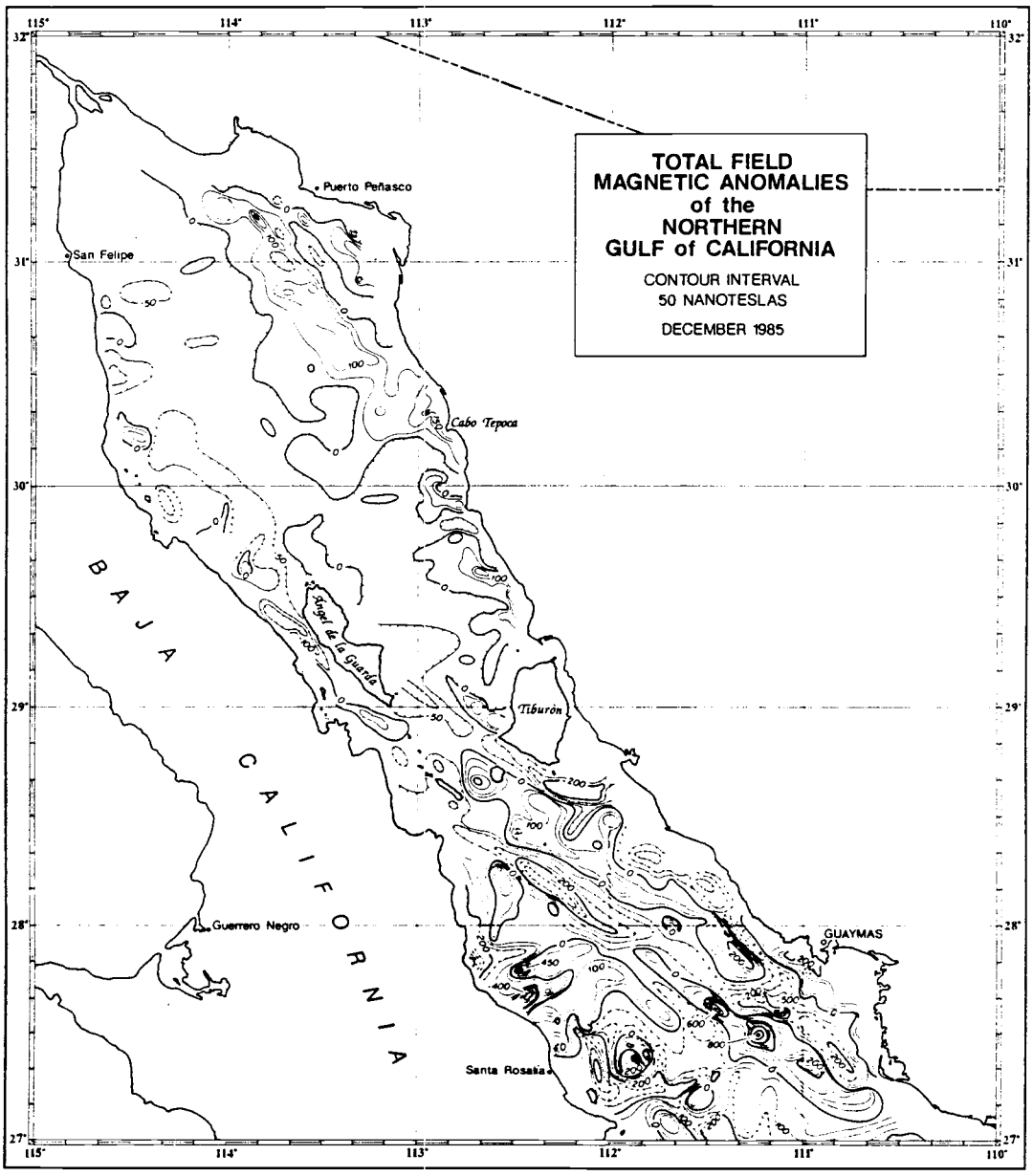

Figure 4. Total-field magnetic anomaly map of the northern Gulf of California

grids share the same characteristics:

North latitude:	32°N
South latitude:	29°N
West longitude:	115°W
East longitude:	112°W
Projection:	Universal Transverse Mercator
Grid size:	256 x 256 km
Grid spacing:	0.5 km

GEOPHYSICAL CROSS-SECTION

In this study, I used constraints from seismic refraction, gravity, magnetic and bathymetric data to construct a crustal and subcrustal model cross-section of the northern Gulf of California. Figure 5 shows the location of the section, which was chosen to accommodate the two-dimensionality required by the modeling program developed by Talwani et al. (1959): its northeast-southwest orientation is approximately normal to the expected strike-slip faults that comprise the en-échelon transform fault zone between the North American and Pacific plates. It was also chosen because the directions of the principal gravity and magnetic anomalies observed in Figures 3 and 4, had the long axis with a northwest-southeast trend. In addition, the location of the profile was selected so that the model could be tied to a seismic refraction line. Thus the cross-section extends 163 km from 30°15'N, 114°50'W in Baja California, to 31°N, 113°W on the Sonora Desert.

Figure 5 shows the seismic refraction lines shot by Phillips (1964). His refraction measurements indicate that the northern Gulf of California is composed of 4 layers: 1.5 km of unconsolidated sediments, 2 km of semiconsolidated sediments, approximately 3 to 8 km (depending on location) of highly variable upper basement, and between 10 and 17 km of lower crust. Layer densities are then obtained using the empirical relation between velocity and density of Ludwig et al. (1970).

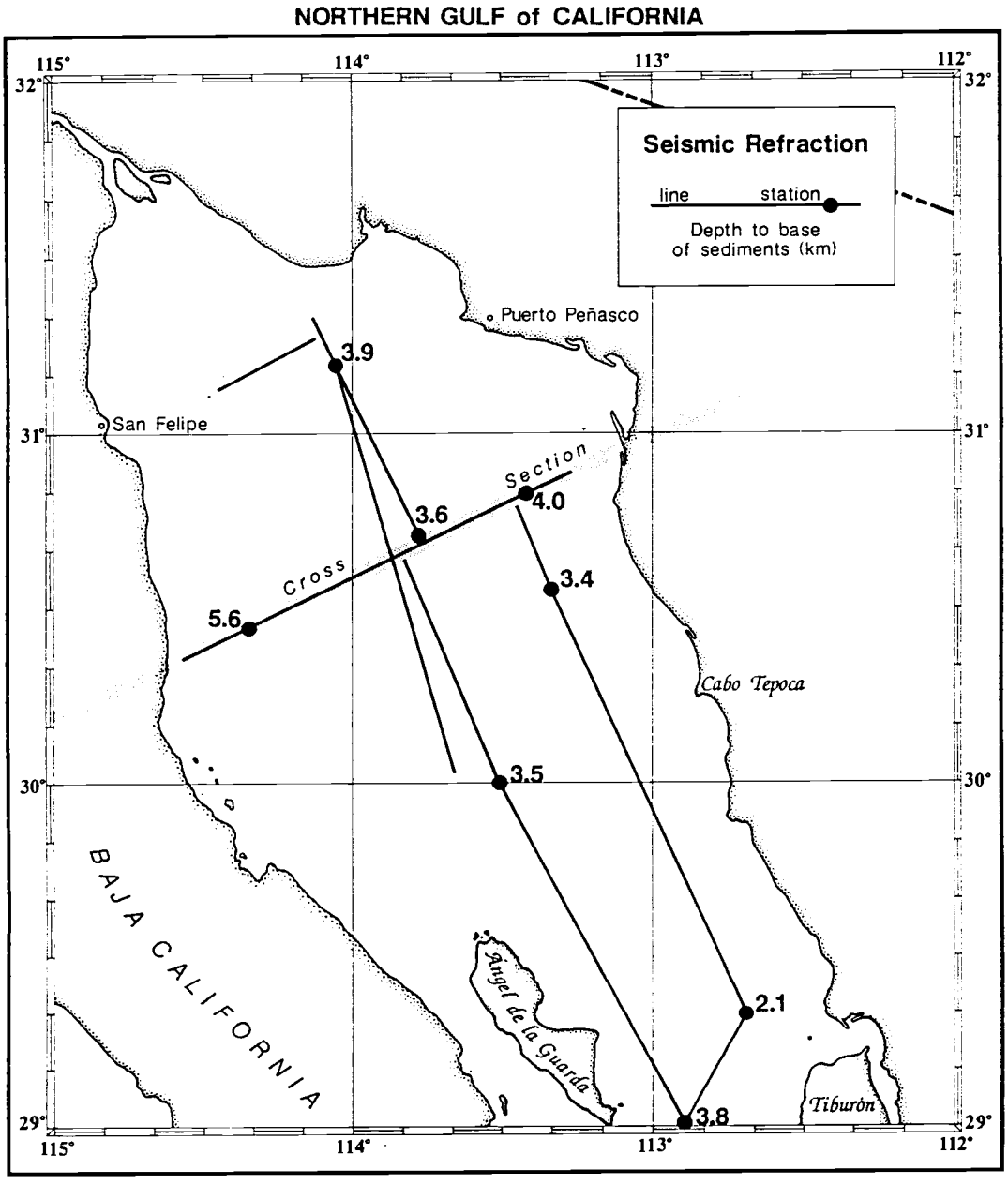

Figure 5. Location of the seismic refraction lines of Phillips(1964), and the cross-section

Based on these results, Phillips proposed that the 20 to 25 km of crust beneath the northern Gulf is similar to the continental rocks that make up the mountain ranges which flank the Gulf. His refraction line between stations 2 and 3 lies directly on my profile and the velocity contrast depths obtained are shown in the model section (Figure 6). The densities shown were computed from the seismic velocities. Table 1 shows the layer thickness (T), seismic velocities (V), and densities (D) for the three seismic refraction stations used to constrain this model, as well as values for a standard oceanic section as computed by Barday (1974).

To provide some constraints on the different magnetic layers present in the substructure, I used the results obtained by spectral analysis of magnetics data conducted by Sanchez-Zamora (1988) to model the tops of the magnetic layers, and the bottom of the deepest magnetic layer.

Figure 6 shows the gravity and magnetic anomaly profiles that constrain the cross-section. The free-air gravity anomaly values to the left of the model start at -25 mGal, decrease slowly to -30 mGal at the center of the first low (which corresponds to the southward continuation of the Consag Basin), then rise to -15 mGal around kilometer 150. The section then crosses the principal anomaly, describing a basin-like shape yielding the lowest value for the section (-40 mGal), as well as the steepest gravity gradient on the

	Station 3			Station 4			Station 2			Average section*		
	T	V	D	T	V	D	T	V	D	T	V	D
Water	0.07			0.08			0.07			4.05		1.03
Layer 1	1.25	1.80	1.80				0.59	1.83	1.80	0.46		2.00
Layer 1a	1.70	3.36	2.25	1.66	2.05	1.95	1.61	2.72	2.20			
Layer 1b	2.62	4.45	2.50	1.81	4.22	2.45	1.96	4.72	2.55			
Layer 2	4.76	5.84	2.65	4.86	5.43	2.60	4.34	5.48	2.60	1.10		2.60
Layer 3		7.22	3.00	9.92	6.80	2.90	12.18	6.46	2.85	4.00		2.90
Moho					8.20	3.30		8.35	3.40			3.32

T = Thickness in km; V = Velocity in km/s; D = Density in gr/cm^3 (Phillips, 1964)

* from Barday (1974)

Table 1. Seismic refraction station velocity data and related densities.

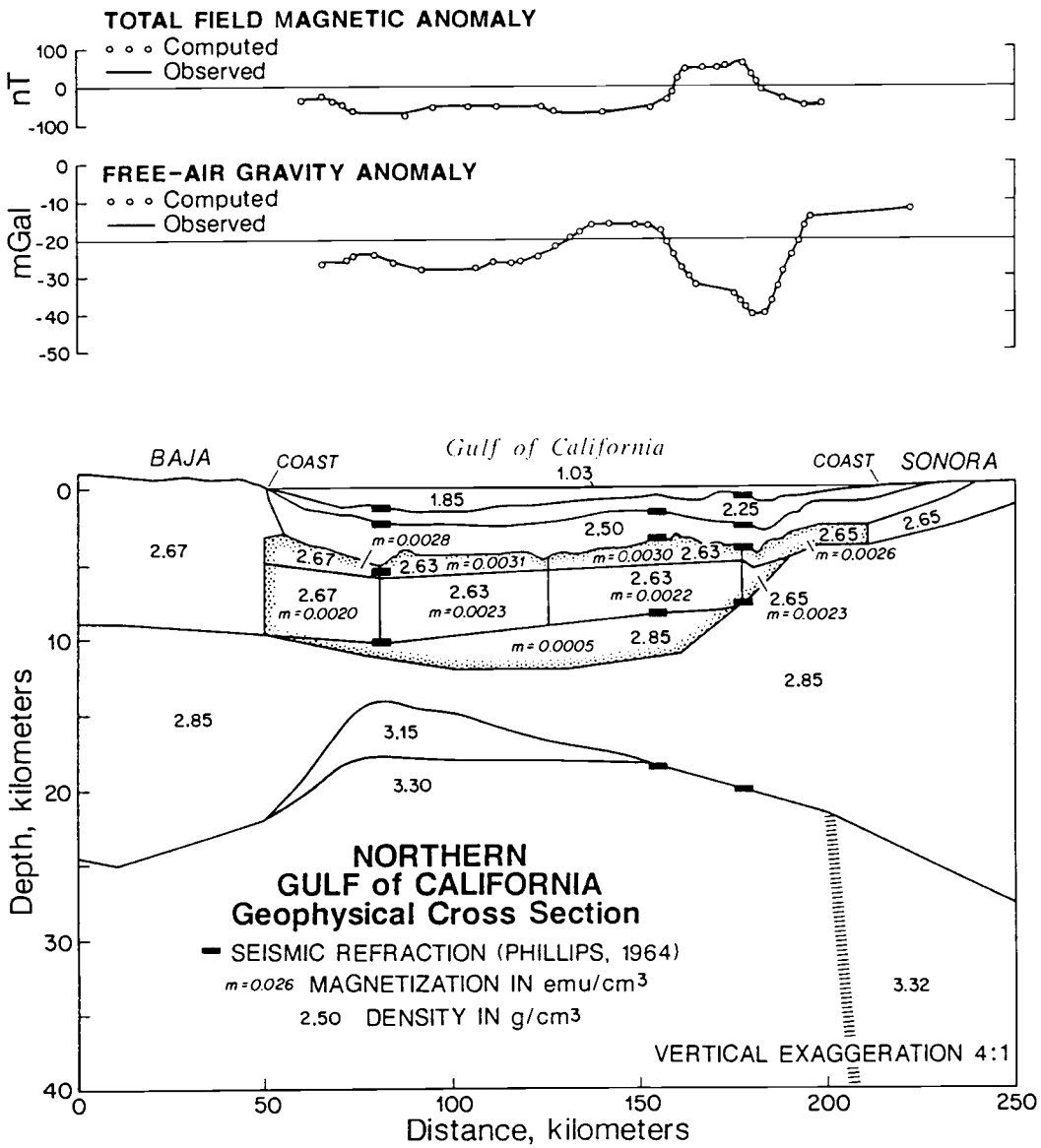

Figure 6. Geophysical cross-section

east side of the basin (4 mGal/km). The anomaly finally rises to -15 mGal at the east end of the model.

The easternmost gravity value (-14 mGal shown in the Sonora region) represents an extrapolation of 3 land gravity measurements available in the vicinity of the section. The total-field magnetic anomaly is remarkably flat in the western two-thirds of the section, presenting almost no variation around an average level of -60 nT; at the same location where the main gravity anomaly occurs, it rises to a 20 km wide anomaly value of 40 nT before decreasing again eastwards to -60 nT.

Assuming that no lateral inhomogeneities exist in the mantle below 50 km, a model of the crustal and subcrustal structure was constructed. Water depths were obtained from bathymetric data obtained concurrently with the gravity and magnetic data, and topographic data for the west and east sides of the section were taken from 1:250,000 contour maps published by the Mexican Direccion General de Estudios del Territorio Nacional (1978). Using the line integral method developed by Talwani et al. (1959), the vertical component of the gravitational acceleration was computed along the profile as being the sum of the gravitational accelerations due to the two-dimensional mass polygons representing the different layers. The results yielded the gravitational acceleration along the profile produced by the model. The free-air gravity anomaly was

then computed by subtracting 6442 mGal from the total acceleration. This is the value computed by Barday (1974) for an average oceanic section 50 km thick, assuming a zero anomaly for this standard section.

The magnetic anomalies were computed using the method of Talwani and Heirtzler (1964), and taking into account the local inclination and declination of the regional field. The values obtained were then reduced to the observed anomalies by subtracting from all computed anomalies the difference between the theoretical and observed magnetic anomaly at the first station.

Iterative adjustment of the shapes of the polygons, and, if necessary, of the corresponding densities during forward modeling, first yields calculated free-air gravity anomalies in agreement with the observed anomalies. Magnetic layers are then introduced to the model to refine it using the comparison between calculated and observed total field magnetic anomalies. The final model incorporated all available constraints. Calculated free-air anomalies fit to within 1 mGal of observed values at each station. Calculated magnetic anomalies match the total field anomalies to within 6 nT.

This geophysical cross-section agrees in total mass with sections previously constructed to the north and south (Plawman, 1978; Calderon, 1978). Since no data were available on land except for topography and a few gravity measurements, only the central

part of the section was modeled in detail. However, mass-columns at the west and east ends of the section are necessary to provide mass balance for the central part of the section. Both ends consist mainly of an upper crustal layer (2.65 to 2.67 g/cm^3), a lower crustal layer (2.85 g/cm^3) and a mantle block (3.30 to 3.32 g/cm^3). Even though the central part of the model exhibits a more complex structure than the land portions of the section, which lack this detailed structuring due to the lack of refraction and other constraining data, it is possible that the central structures do not extend landward because of the translational motion along the edges of the Gulf caused by the San Pedro Martir and the Cerro Prieto fault zones. The models developed by Calderon (1978) across the central part of the Gulf display the same general mass distribution along the profile.

The model shows a relatively thin 20 km of crust beneath the Gulf. This thickens to 25 km beneath Baja California and makes a transition to continental-crust beneath the Mexican mainland, dipping progressively to 35 km. The substructure of the Gulf is asymmetrical with respect to its central axis. While the upper crustal layer gets shallower to the east, a layer with a density of 3.15 g/cm^3 occurs beneath the southwestern side of the Gulf between the mantle and the lower crust. This anomalous structure has also been noted by Plawman (1978) and by Fuis et al. (1984) in the Imperial Valley north of this section. It was also shown by Calderon (1978), who described the same low density anomalous mantle in his models south of this section. This sub-basement is required to compensate

the gravitational attraction caused by the westward dipping of the main crustal layer, and also to fit the refraction data.

The lower crustal layer exhibits a density of 2.85 g/cm^3. The seismic velocities recorded for this layer (5.5 to 5.8 km/s) are similar to those found for extrusive basalt or metabasalt by Christensen and Salisbury (1975), who showed that the velocity of greenschist-facies metabasalt under normal conditions (1 kbar, room temperature, water saturated) range from 5.3 to 6.3 km/s. The rock layers composing the upper crustal layer have densities between 2.63 and 2.67 g/cm^3, with the lower densities located beneath the Gulf itself. These layers also display magnetizations of .0005 to .0030 emu/cm^3. These values correspond to those of serpentinite, which is known to occur in the Franciscan complex north of the area (Plawman, 1978). The slight differences in modelled magnetization, which were necessary to obtain a good fit between the calculated and observed magnetic data, may reflect variations caused by hydrothermal processes associated with rifting.

Sediment densities normally increase continuously downward because of the compaction process. The three layers of sediments shown in the model, with densities ranging from 1.85 to 2.50 g/cm^3 represent averages for each layer. Because the seismic refraction data show a seismic boundary between two layers, it can be expected that the composition of each layer is different. For example, the lower layer of the sedimentary fill is quite dense (2.50 g/cm^3), and is

probably somewhat metamorphosed. Metamorphism of sediment has been observed in drill cores from this area (Elders et al., 1972). The sediment-hardrock interface however is very well defined from seismic refraction, gravity and magnetic modeling. Its roughness can perhaps be explained by the presence of strike-slip faults throughout the area. This is particularly visible at the east end of the model where the sediment layer as well as the basement interface show signs of the disturbance created by the Cerro Prieto fault zone.

WERNER DECONVOLUTION

Basic concept

The Werner deconvolution method (Werner, 1953) is an automated interpretation method of magnetic profiles based on the assumption that the source of the anomalies can be approximated by a series of thin dikes. It leads to the possible linearization of complex nonlinear magnetic problems.

Although Werner first published his paper in 1953, it was not until 1968 that this method began to be used extensively by geophysicists as part of a routine automated magnetic interpretation system. Hartman et al. (1971) were the first to describe its application to field problems. Jain (1976) demonstrated the theory behind it in more detail by using synthetic models. Stanley (1977) presented a manual interpretation procedure based on the thin dike and interface relationship. More recently, Ku and Sharp (1983) summarized the current state of knowledge by applying the Werner deconvolution to both synthetic models and real field data and using a statistical decision approach.

Although the initial use of the Werner deconvolution method was restricted to thin dike solutions using the total field as input data, I will show that the horizontal gradient of the magnetic field

can be used to give solutions that can be indicative of the edge of a thick block interface. By using both types of determination, the Werner deconvolution method can lead to a good approximation of the position of the dike or block edge, as well as its depth, dip angle and magnetic susceptibility.

Consider the magnetic anomaly created by a two-dimensional thin dike (Figure 7). In order to realize a good approximation of projecting the anomaly on a 2-D profile, I choose the x-axis to be perpendicular to the strike of the dike, the y-axis parallel to the strike, and the z-axis vertical, and further assume that the dike extends to infinity in both the y and z directions.

The computed anomaly for such a dike can be calculated using the following equations from Talwani and Heirtzler (1964).

The vertical magnetic anomaly is given by:

$$VMAG\ (x, z) = 2 \iint \left[J_x \frac{2(x'-x)(z'-z)}{R^4} + J_z \frac{2(z'-z)^2 - R^2}{R^4} \right] dx'\ dz'$$

where

$$R = \sqrt{(x' - x)^2 + (z' - z)^2}$$

and

$J = (J_x, J_z)$ is the polarization vector composed by the induced and the remnant magnetizations.

The horizontal magnetic anomaly can be expressed as:

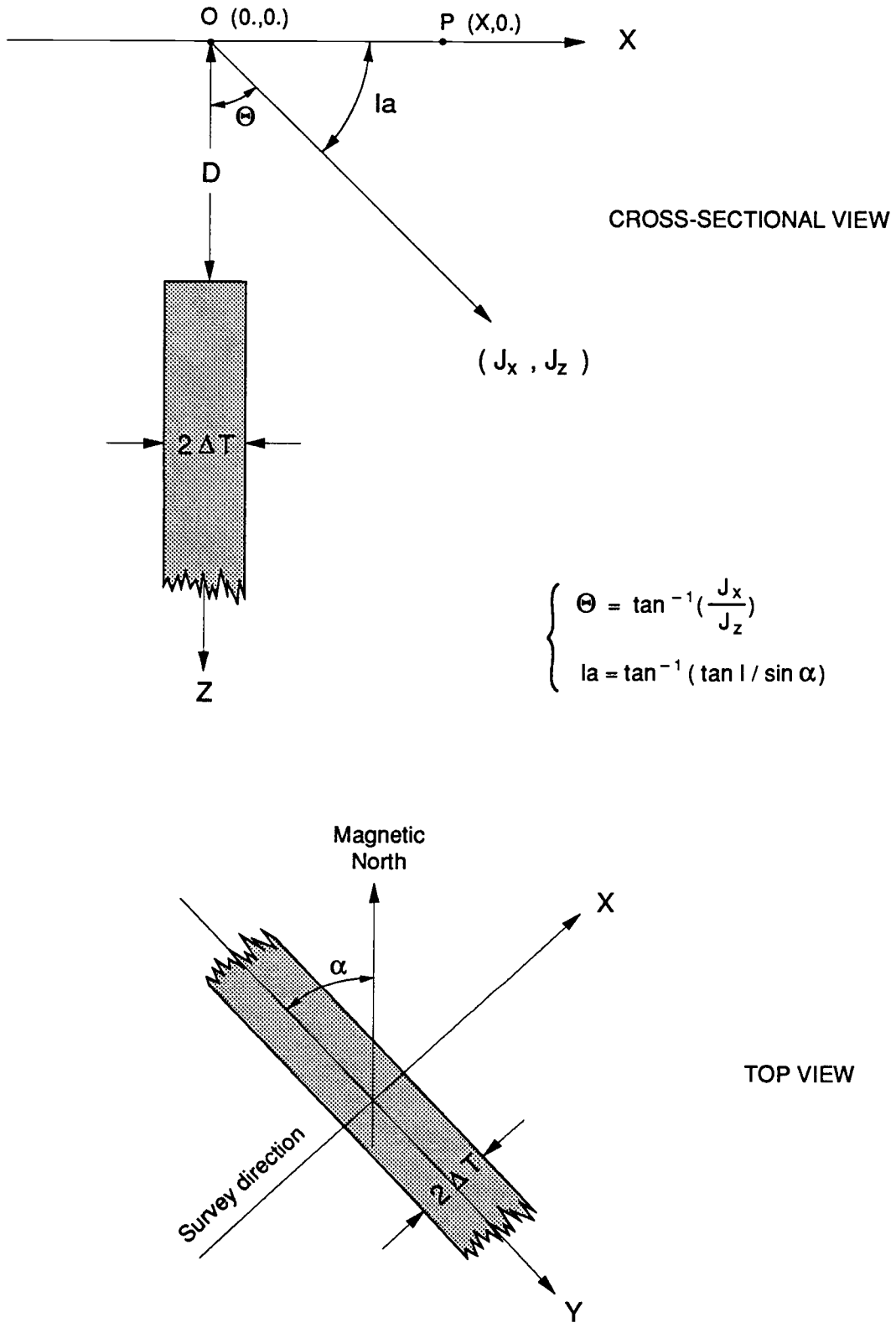

Figure 7. Parameters of a thin vertical dike

$$\text{HMAG}(x, z) = 2 \iint \left[J_x \frac{2(x'-x)^2 - R^2}{R^4} + J_z \frac{2(x'-x)(z'-z)}{R^4} \right] dx'\, dz'$$

Combining both equations leads to the expression of the total magnetic anomaly for a thin dike:

$$\text{TMAG}(x, z) = \text{HMAG}(x, z) \cos I \sin \alpha + \text{VMAG}(x, z) \sin I$$

where I is the magnetic inclination of the main field F, α is the strike of the dike as measured from magnetic north, positive counterclockwise.

Let D be the depth of the top of the dike and $2\Delta T$ its thickness. In the case of a thin dike, I will be able to make some simplifications to the above equations which will ultimately lead to a straight-forward integration. As the thickness becomes small compared to the depth, ($\Delta T \ll D$), I can write:

$$\text{VMAG}(x, z) = 2 \int_{D}^{\infty} \int_{-\Delta T}^{\Delta T} \left[J_x \frac{2(x'-x)(z'-z)}{R^4} + J_z \frac{2(z'-z)^2 - R^2}{R^4} \right] dx'\, dz'$$

which, by further assuming that the observation point is at sea level, can be approximated to:

$$\text{VMAG}(x, 0) \cong 2 \cdot 2\Delta T \left(J_x \int_{D}^{\infty} \frac{-2xz'}{R^4} dz' + J_z \int_{D}^{\infty} \frac{2z'^2 - R^2}{R^4} dz' \right)$$

Finally I obtain:

$$VMAG\ (x, 0) = 2\Delta T \frac{J_z D - J_x x}{x^2 + D^2}$$

Similarly, the horizontal field magnetic anomaly can be expressed as:

$$HMAG\ (x, 0) = -2\Delta T \frac{J_x D + J_z x}{x^2 + D^2}$$

Finally, I have

$$TMAG\ (x, 0) = HMAG\ (x, 0) \cos I \sin \alpha + VMAG\ (x, 0) \sin I$$

$$= \frac{Ax + BD}{x^2 + D^2} \qquad (1)$$

where $A = -2\Delta T(J_x \sin I + J_z \cos I \sin \alpha)$

$$B = -2\Delta T(-J_x \cos I \sin \alpha + J_z \sin I)$$

The polarization vector can be expressed in terms of A and B:

$$J_x = \frac{-BV_x - AV_z}{2\Delta T(V_x^2 + V_z^2)} \qquad (2)$$

and

$$J_z = \frac{-AV_x + BV_z}{2\Delta T(V_x^2 + V_z^2)} \qquad (3)$$

with

$$V_x = \cos I \sin \alpha$$

$$V_z = \sin I$$

Note that equation (1) is valid only when the position of the top of the dike is at the location (0,D). For an arbitrary horizontal position, this equation should be rewritten as:

$$TMAG(x, 0) = \frac{A(x - x_o) + BD}{(x - x_o)^2 + D^2} \qquad (4)$$

This represents the total field anomaly generated by the dike alone. Now, I will take into consideration the main dipole field and the regional field gradient. I express this gradient as a polynomial of second order. Hence, the total field is now expressed as:

$$TMAG(x, 0) = \frac{A(x - x_o) + BD}{(x - x_o)^2 + D^2} + C_o + C_1 x + C_2 x^2 \qquad (5)$$

Upon rearranging, I have:

$$a_o + a_1 x + a_2 x^2 + a_3 x^3 + a_4 x^4 + b_o TMAG + b_1 x\ TMAG$$

$$= x^2\ TMAG$$

where

$$a_o = - A x_o + B D + C_o D^2 + x_o^2 C_o$$

$$a_1 = A - 2 C_o x_o + C_1 D^2 + C_1 x_o^2$$

$$a_2 = C_o - 2 C_1 x_o + C_2 x_o^2 + C_2 D^2$$

$$a_3 = C_1 - 2 x_o C_2$$

$$a_4 = C_2$$

$$b_o = - x_o^2 - D^2$$

$$b_1 = 2 x_o$$

I now have one equation with seven unknowns: a_0, a_1, a_2, a_3, a_4, b_0 and b_1 . Thus, if I can know the values of the total field at seven different points, I will possess a solvable system of equations.

I choose such 7 points so that they are equally spaced in the x–direction where x is the horizontal location of the fourth point in the series and Δx the sample spacing between two consecutive points.

I have

$$
\begin{aligned}
TM1 &= TMAG(x - 3\Delta x, 0) \\
TM2 &= TMAG(x - 2\Delta x, 0) \\
TM3 &= TMAG(x - \Delta x, 0) \\
TM4 &= TMAG(x , 0) \\
TM5 &= TMAG(x + 1\Delta x, 0) \\
TM6 &= TMAG(x + 2\Delta x, 0) \\
TM7 &= TMAG(x + 3\Delta x, 0)
\end{aligned}
$$

I can now rewrite this system in dimension-less form by equating Δx to unity:

$$
\begin{bmatrix}
1 & -3 & 9 & -27 & 81 & TM1 & -3TM1 \\
1 & -2 & 4 & -8 & 16 & TM2 & -2TM2 \\
1 & -1 & 1 & -1 & 1 & TM3 & -TM3 \\
1 & 0 & 0 & 0 & 0 & TM4 & 0 \\
1 & 1 & 1 & 1 & 1 & TM5 & TM5 \\
1 & 2 & 4 & 8 & 16 & TM6 & 2TM6 \\
1 & 3 & 9 & 27 & 81 & TM7 & 3TM7
\end{bmatrix}
\begin{bmatrix} a_0 \\ a_1 \\ a_2 \\ a_3 \\ a_4 \\ b_0 \\ b_1 \end{bmatrix}
=
\begin{bmatrix} 9TM1 \\ 4TM2 \\ TM3 \\ 0 \\ TM5 \\ 4TM6 \\ 9TM7 \end{bmatrix}
$$

Solving the simultaneous equations of this system is a simple even-determined linear problem. One method would be to use a linear operator as Werner originally proposed. In this study I will apply a matrix inversion routine, using a Gauss-Jordan reduction method (Menke, 1984).

In terms of the unknowns,

$$x_0 = b_1/2$$

$$D = \sqrt{-b_0 - x_0^2}$$

$$C_2 = a_4$$

$$C_1 = a_3 + 2 x_0 C_2$$

$$C_0 = a_2 + 2 C_1 x_0 - C_2 x_0^2 - C_2 D^2$$

$$A = a_1 + 2 C_0 x_0 - C_1 D^2 - C_2 x_0^2$$

$$B = \frac{1}{D} (a_0 + A x_0 - C_0 D^2 - C_0 x_0^2)$$

Replacing A and B with their expression in equations (1) and (2), I obtain the values for the polarization vector (J_x, J_z), which in turn leads to the computation of the magnetic susceptibility and dip angle of the dike. Thus, in real physical dimensions, the dike parameters expressed in terms of the sample spacing Δx are

$$\text{horizontal position} = 0.5\, b_1 \Delta x + x$$

$$\text{depth} = \sqrt{-b_0 - 0.25\, b_1^2\, \Delta x} \qquad (6)$$

$$\text{magnetic susceptibility} = \frac{\sqrt{J_x^2 + J_z^2}}{|F|}\,\Delta x$$

$$\text{dip angle} = \tan^{-1}\left(\frac{J_x}{J_z}\right) + I_a$$

At this point I can make two observations related to the physical meaning of these equations.

First, since I want the computed value of the depth to be part of the physical world, I cannot allow it to have any imaginary components. Thus the constraint from equation (6):

$$-b_o - 0.25\, b_1^2 > 0$$

This constraint is related to the choice of the length of the Werner operator with respect to the length of the anomaly. If the operator is too small, only a short and therefore quasi-linear portion of the anomaly will be considered in the inversion process, leading to the computation of a depth greater than reality. Then, if the operator is much larger than the average anomaly, several peaks will be included in the portion of the anomaly under deconvolution, and the inversion will not yield true results or will not satisfy the above constraint. A large operator can also introduce aliasing: the sampling of anomalies having a wavelength lower than that of the operator could cause the inversion process to yield solutions representing sources that generate an anomaly broader than in reality. Therefore the choice of the length of the operator should be somewhere between those two extremes. Ideally, that length should be such that

it is large enough to see the variations in the curvature of the anomaly (thus satisfying equation (6)) but small enough to cover only a single peak (leading to a reliable computational result).

The second observation comes from the computation of the magnetic susceptibility σ. Equations (2) and (3) require that I must assume the thickness of the dike in order to compute the polarization vector. Hence the magnetic susceptibility is the least reliable of the computed parameters. Indeed, since the thickness of any of the dikes forming the anomaly are assumed to be constant through the whole computation, the computed susceptibility can yield values greatly different from the real value. This is a problem very often encountered in potential field studies: for example, we can only resolve the product of density and thickness in gravity problems, or the product of the depth to the magnetic layer and the Curie temperature in Curie-point analysis problems.

The utility of the Werner deconvolution technique is further extended by applying it to the horizontal gradient of the total field as well as to the total field itself, since the horizontal gradient of the total field caused by the edge of a thick interface body is equivalent to the total field caused by a thin dike (Ku and Sharp, 1983). This is easily demonstrated if the thick interface body is visualized as being composed of a infinite number of infinitesimally thin dikes dipping parallel to the interface. The anomaly created by such a body is equal to the integration over horizontal distance of the thin dike

anomaly. Taking the gradient cancels the integration, hence the equivalence.

In the case where solutions interpreted as edges of interfaces or faults are desired, the horizontal gradient is extracted from the profile by applying the Lagrangian interpolation formula for seven points (Gerald et al, 1984), since this is the number of consecutive data points I will be using for the Werner operator.

$$\frac{d}{dx}\mathrm{TMAG}(x) = \frac{(x-x_2)(x-x_3)\ldots(x-x_7)}{(x_1-x_2)(x_1-x_3)\ldots(x_1-x_7)}\ \mathrm{TM1}$$

$$+\ \frac{(x-x_1)(x-x_3)\ldots(x-x_7)}{(x_2-x_1)(x_2-x_3)\ldots(x_2-x_7)}\ \mathrm{TM2}$$

$$+\ldots+\frac{(x-x_1)(x-x_2)\ldots(x-x_6)}{(x_7-x_1)(x_7-x_2)\ldots(x_7-x_6)}\ \mathrm{TM7}$$

Since all of this is accomplished in dimensionless space with equally spaced samples, this formula is greatly simplified when evaluated at $x = x_4$, with $x_2-x_1 = x_3-x_2 = \ldots = x_7-x_6 = 1.0$:

$$\mathrm{HMAG}(x_4) = \frac{d}{dx}\mathrm{TMAG}(x_4)$$

$$= (\mathrm{TM7}-\mathrm{TM1})/60 - (\mathrm{TM6}-\mathrm{TM2})*3/20 + (\mathrm{TM5}-\mathrm{TM3})*3/4$$

Following the same procedure as before, but this time using the computed horizontal gradient as the input, solutions can be obtained which may be interpreted as the edges of thick interfaces.

Synthetic Models

In order to test the deconvolution technique, I will construct some models. Since the deconvolution provides a very close

approximation when the geologic body is an infinitely long thin dike (when using total field anomalies) or the edge of a layer (when using the horizontal gradient), these kind of bodies will be used in my models.

First I consider an ideal thin dike as shown in Figure 8. The dike is 1 km wide, 5 km deep and the sample spacing between computed magnetic anomalies is .5 km. The total magnetic anomaly caused by the dike is about 30 km wide. As explained before, it is important to correctly evaluate the width factor. The Werner operator that I chose for this dike was .8 which gives a moving window of about 25 km. Since the sample spacing is .5 km and the moving window is composed by 7 equidistant locations, the spacing between two consecutive values is about 3.5 km or 7 samples.

As the Werner window sweeps from left to right across the profile, increasing its location by .5 km each time, I obtain a series of solutions whose depths are indicated by cross symbols, and dip angles by straight line segments. Since the formula used for the Werner deconvolution is applied here to a vertical dike, the total field solutions yield dip angles which are more or less perpendicular to the part of the curve straddled by the Werner window. If this could be seen in time sequence, it would be noticed that the dip angles rotate clockwise from dipping to the right to dipping to the left in accordance with the normal direction of the total field curve.

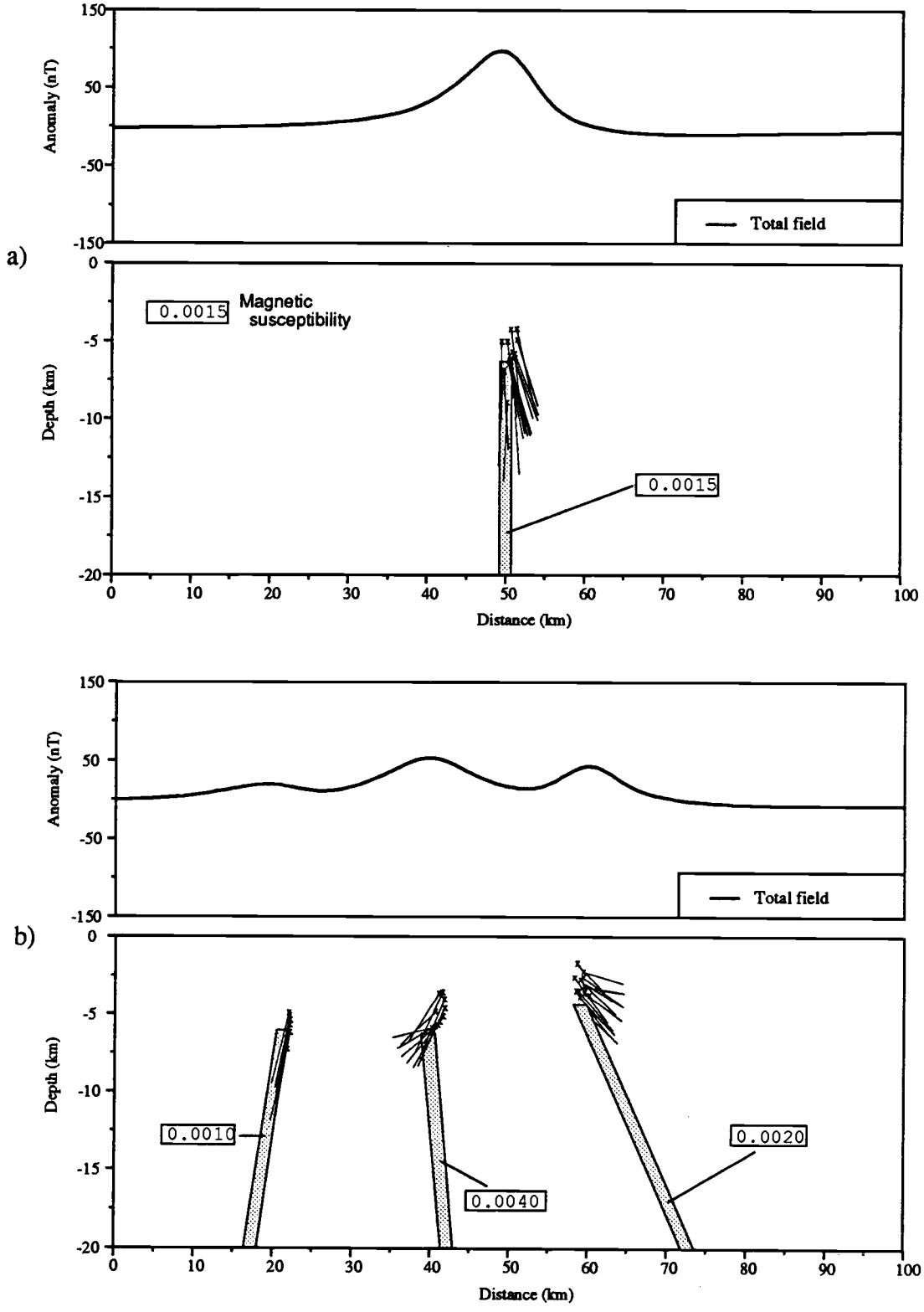

Figure 8. Models and Werner solutions using the total-field magnetic anomaly method:
a) one-dike model
b) three-dike model

However, because the seven-point operator I am using takes into account the regional trend at each evaluation, this side effect is greatly reduced. This would not be the case if I were to use a four-point operator.

Observe in Figure 8a that the Werner solution yields a good computation with respect to horizontal position, depth and dip angle. Computed susceptibility is greater than the true susceptibility by a factor of 10. This is the least resolved of the computed parameters. Not all the computed estimations are shown on figure 8a. Solutions on a profile can typically be grouped into "clusters" that appear near the location of true features. But estimations are also computed when the skewness of the anomaly curve matches a possible solution. This calls for a rejection criteria in order to discard nonexistent solutions. Here I will reject estimations that are more than one standard deviation from the mean of the horizontal location of a cluster of solutions.

Figure 8b represents a more realistic problem where several dikes coexist on the profile. The width of the isolated anomaly due to any one of the dikes is still about 30 km. However the contribution of neighboring dikes changes the shape of the curve representing each dike. Three thin dikes are featured in this model, with the top of each dike separated by 20 km in horizontal direction. The true susceptibility range from 0.0010 to 0.0040 emu/cm^3. The

leftmost dike is the best resolved, with excellent solutions for horizontal location, depth and dip angle. A look at the two other dikes shows that in both cases the horizontal location is accurately computed, while the depths yield values shallower than the true depths, but still within an acceptable range. However, it can be seen that the dip angle computed for the middle dike differs considerably from the actual angle, showing in fact a dip opposite of what the true one is.

To test the efficiency of the horizontal gradient method, I construct two models dealing with edges of thick interfaces. I will use blocks having different magnetizations representative of actual material.

In Figure 9a, I consider a magnetized slab lying at a depth of 6 km, composed of materials of different susceptibility, 0.0015 and 0.0025 emu/cm^3. The shape of the anomaly curve this time reflects the changes occurring in lateral magnetization. Starting at -20 nT on the left of the profile, the magnetic total-field anomaly increases to 70 nT when it crosses the first interface, reaches 100 nT in the middle of the slab where an increase of magnetization occurs in the material, and then decreases to about -50 nT at the second interface. Estimating the width of the average anomaly in this case is more difficult. If I were to operate the Werner deconvolution on the total field, looking for dike-like solutions, the anomaly size would look about 40 km long, as there are two main contributions to the curve. Since I will use the horizontal gradient of the anomaly, dealing with

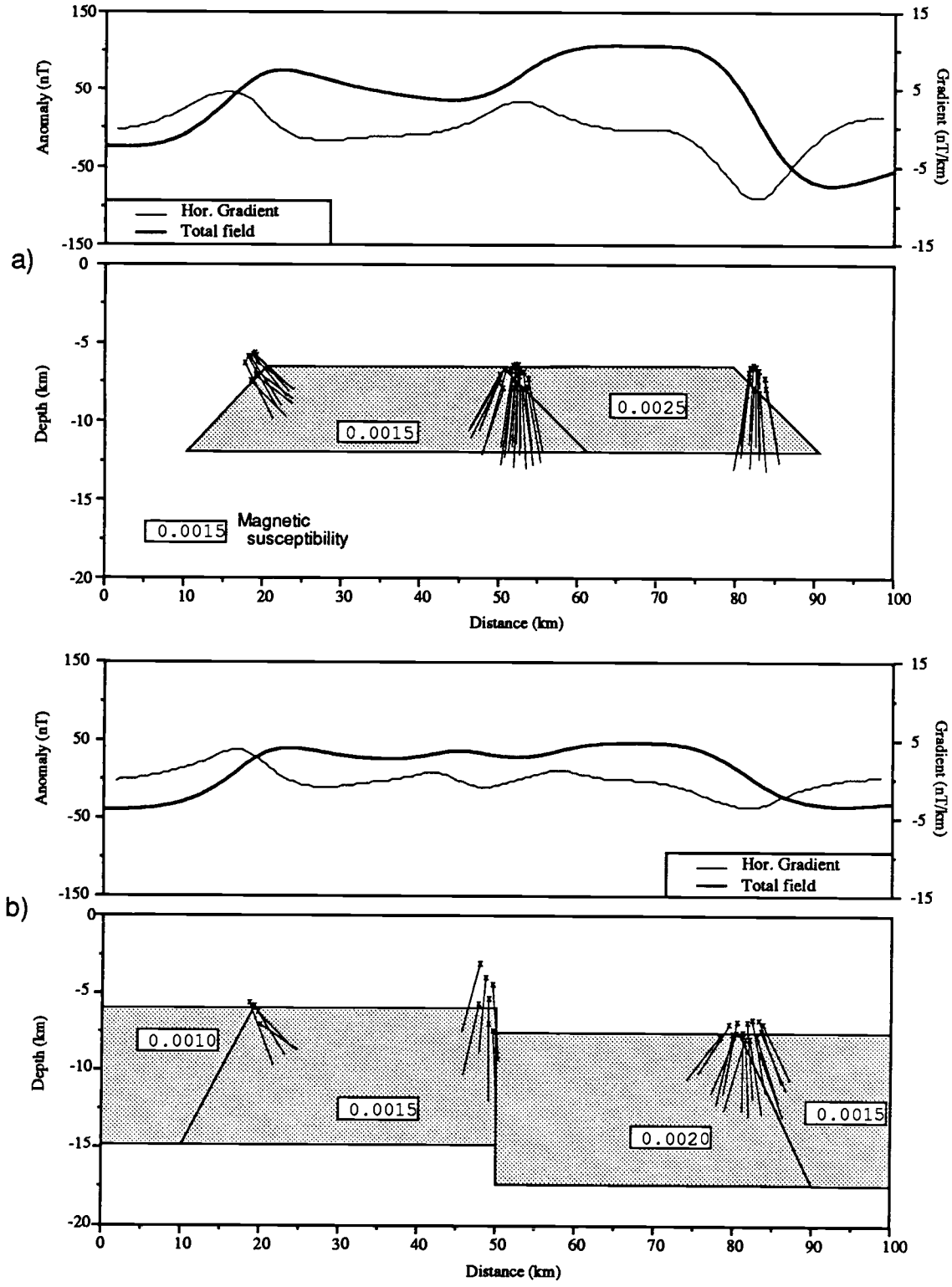

Figure 9. Models and Werner solutions using the horizontal gradient of the magnetic anomaly method:
a) two-block model
b) four-block model

interfaces, I therefore will use the average width that was used before, 30 km. The clusters of solutions agree quite well with the model with respect to horizontal location and depth. However, the dip angle as computed for the first interface is opposite in sign to the real dip angle. Ku and Sharp (1983) explain this kind of result by deriving the equations for the horizontal gradient solution in two different ways. Whenever the interface body extends to infinity in the negative x-axis direction, the dip angle computed from the horizontal gradient is the same as the true dip angle of the interface. However, if the body extends to infinity in a positive x-axis direction, the sign of the computed dip angle is the opposite of the true dip angle. In this case a computation involving the total field is helpful since the dip angle computed for a dike-like solution would be correct.

Though the other parameters of the dike are of no interest, the dip angle provides a clue in distinguishing between the two possible solutions.

Figure 9b involves a more realistic model. It includes four blocks of different susceptibility, ranging from 0.0010 to 0.0020 emu/cm^3. The left and the right interfaces are representative of a strike-slip fault, with a slight change in susceptibility on each side of the fault. The central interface represents a fault involving both a vertical displacement and also a change in susceptibility. Note the shape of the anomaly across this profile. The interfaces on both sides

of the model are well characterized and produce a well defined offset in the observed magnetic anomaly. It would be easy to compute the inversion via a different method, for example, the midpoint method (Radhakrishna Murthy, 1985). However, the central interface provides almost no variation in the total field anomaly, making it an excellent candidate for the Werner deconvolution method.

The results of this model agree with those from the previous models — a good estimation of the horizontal location and the depth of the top edges of the interfaces. Although the dip angle computed to the first interface is subject to the same verification as before from a total-field solution, the second and third interfaces yield good solutions with respect to the dip angle. This is especially true of the central fault, where the computed and actual dip angle values coincide. The depths calculated for this fault are a little scattered (from 3 to 7 km) and their mean seems to indicate a solution for the topmost edge of the left block (6 km) while the downthrown right block has its topmost edge at 8 km. This is a common problem in the analysis of magnetic anomalies. When two geologic features (body interfaces, dikes, ...) are present at the same location but at different depths, the shallower feature contributes almost exclusively to the generation of an anomaly.

These synthetic models demonstrate that the Werner deconvolution method yields good estimations of the location and depth of dikes or edges of thick interface bodies. I will next apply the method to real data.

The northern Gulf of California Fault Pattern

The northern Gulf of California is an appropriate area in which to apply the Werner deconvolution method because the thick layers of sediments, and the low amplitude of the anomalies makes it difficult to apply other more commonly used methods. In order to define the fault pattern here, I examined the six profiles shown in Figure 10.

These profiles were chosen to be approximately perpendicular to the main linear magnetic anomalies, which have a general NW-SE trend. The profiles were extracted from the grid containing the total field anomaly. The distance between the profiles is approximately 25 km. Since the profiles were extracted from a grid, the magnetic anomalies are equally spaced along each profile. This was not true on the previous synthetic models. There, a model was first defined, then its theoretical anomaly computed by forward modeling following the method of Talwani and Heirtzler, then the anomaly was splined to provide a uniformly spaced data set. Depending on the kind of algorithm used for splining, this operation can also act like a low-pass filter, eliminating or modifying some data. But this smoothing operation, which is also indirectly performed when extracting data from a grid, has been proven to have a beneficial effect on the model studies, by eliminating low-level noise and thereby reducing the number of inconsistent solutions.

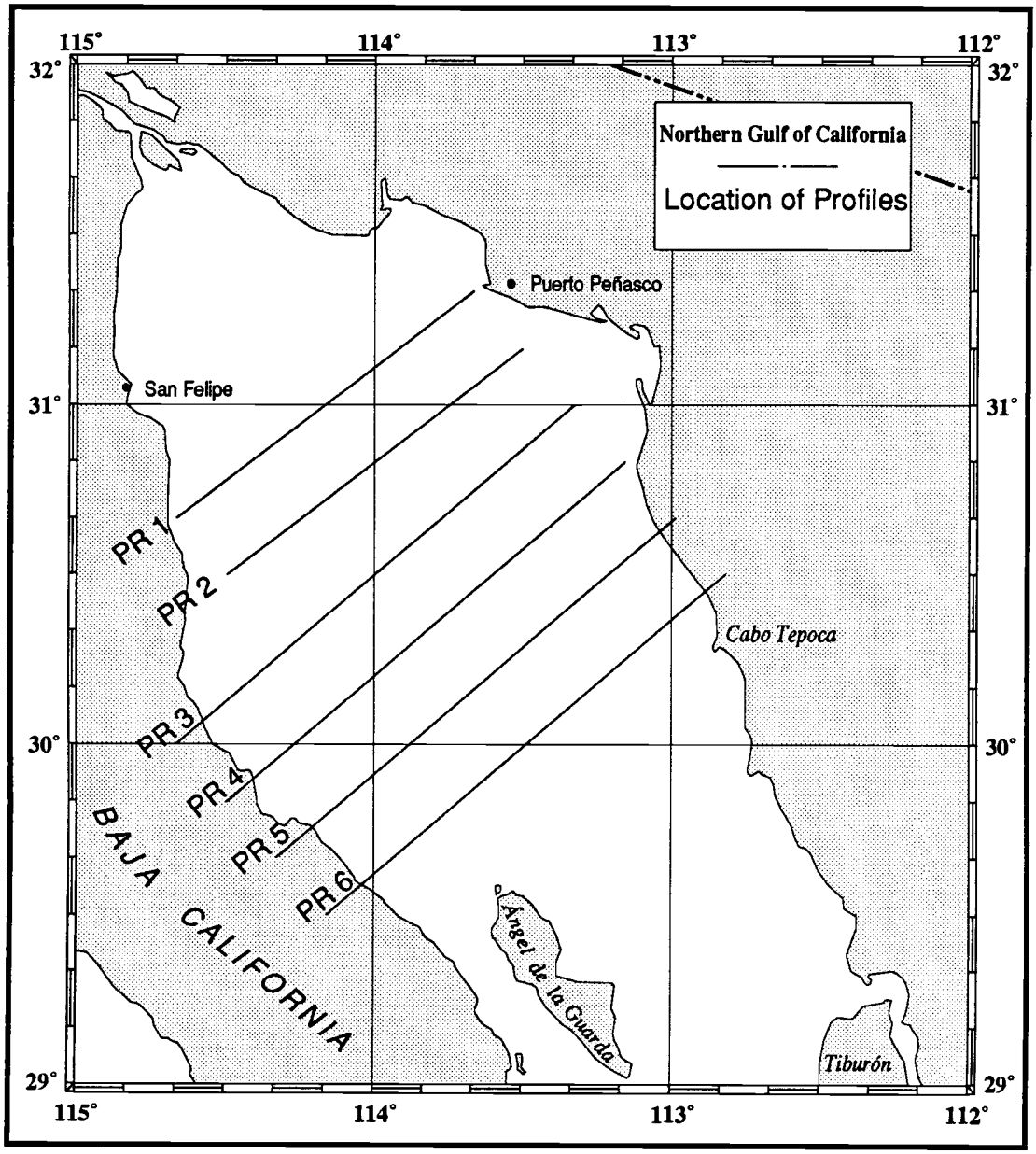

Figure 10. Location of Magnetic Profiles PR1 to PR6.

The solution given by the deconvolution for each of these profiles is shown on Figures 11 through 13.

The length of the average magnetic anomaly for all these profiles was estimated at 30 km. Several runs were made for each profile for various values of the Werner operator between .5 and .9. The solutions shown here correspond to an operator of .8. A cluster of estimates then determines a valid solution. After removing all estimates more than one standard deviation in horizontal location, the mean of the four parameters is computed again and shown in Table 2.

Profile	Location (km)	Depth (km)	Susceptibility (emu)	Dip angle (degrees)
PR1				
	35	4	0.00058	105
	66	2	0.00047	7
PR2				
	35	-	0.00124	-
	66	5	0.00039	130
	100	5	0.00223	53
PR3				
	39	6	0.00143	93
	64	2	0.00007	55
	81	3	0.00011	34
	121	4	0.00037	92
PR4				
	35	5	0.00089	114
	43	8	0.00182	111
	99	8	0.00056	49
	140	7	0.00095	-
PR6				
	64	-	0.00029	42
	80	5	0.00051	123
	134	4	0.00029	88

Table 2. Werner solutions for profiles PR1 to PR6.

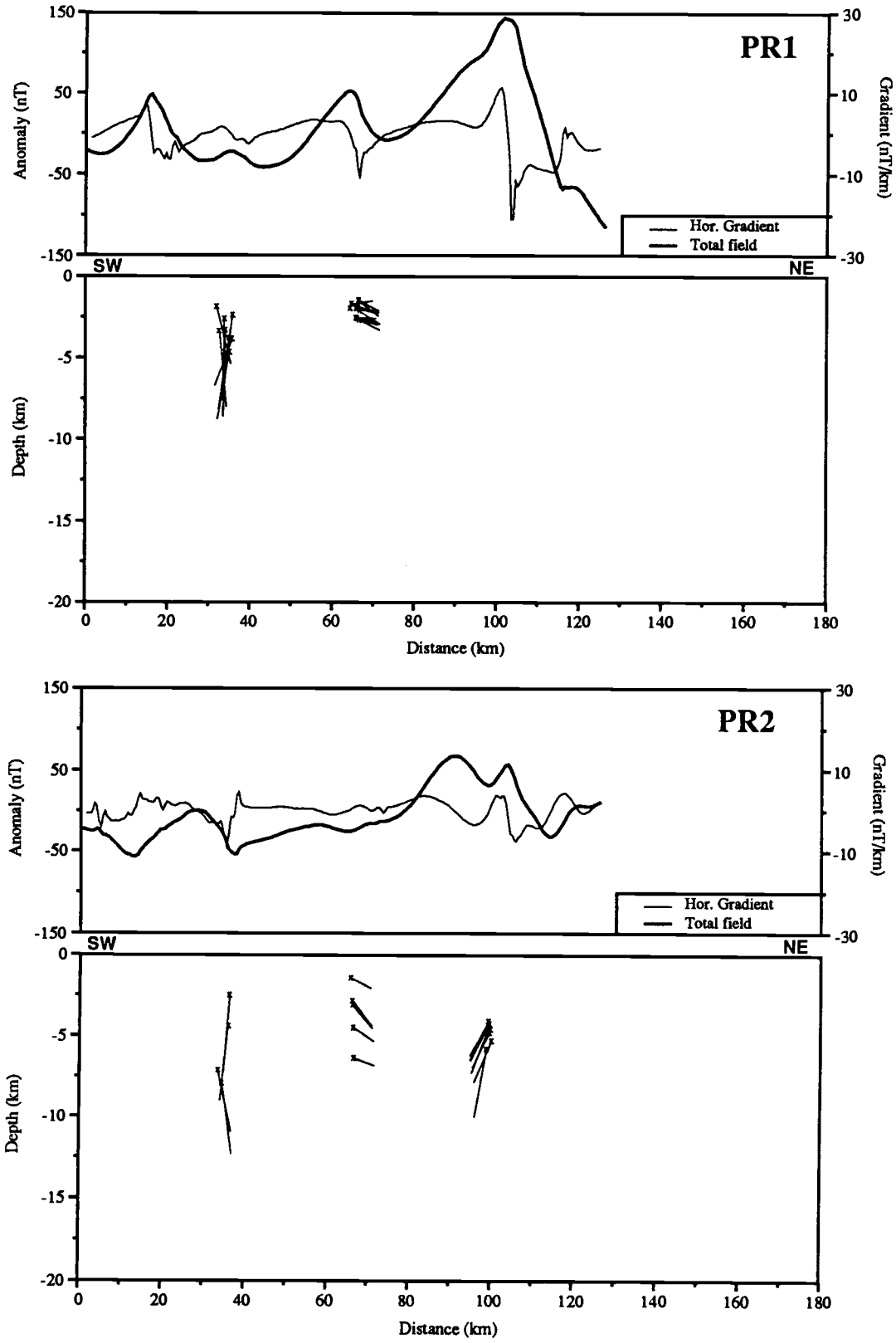

Figure 11. Magnetic anomalies and Werner solutions of profiles PR1 and PR2.

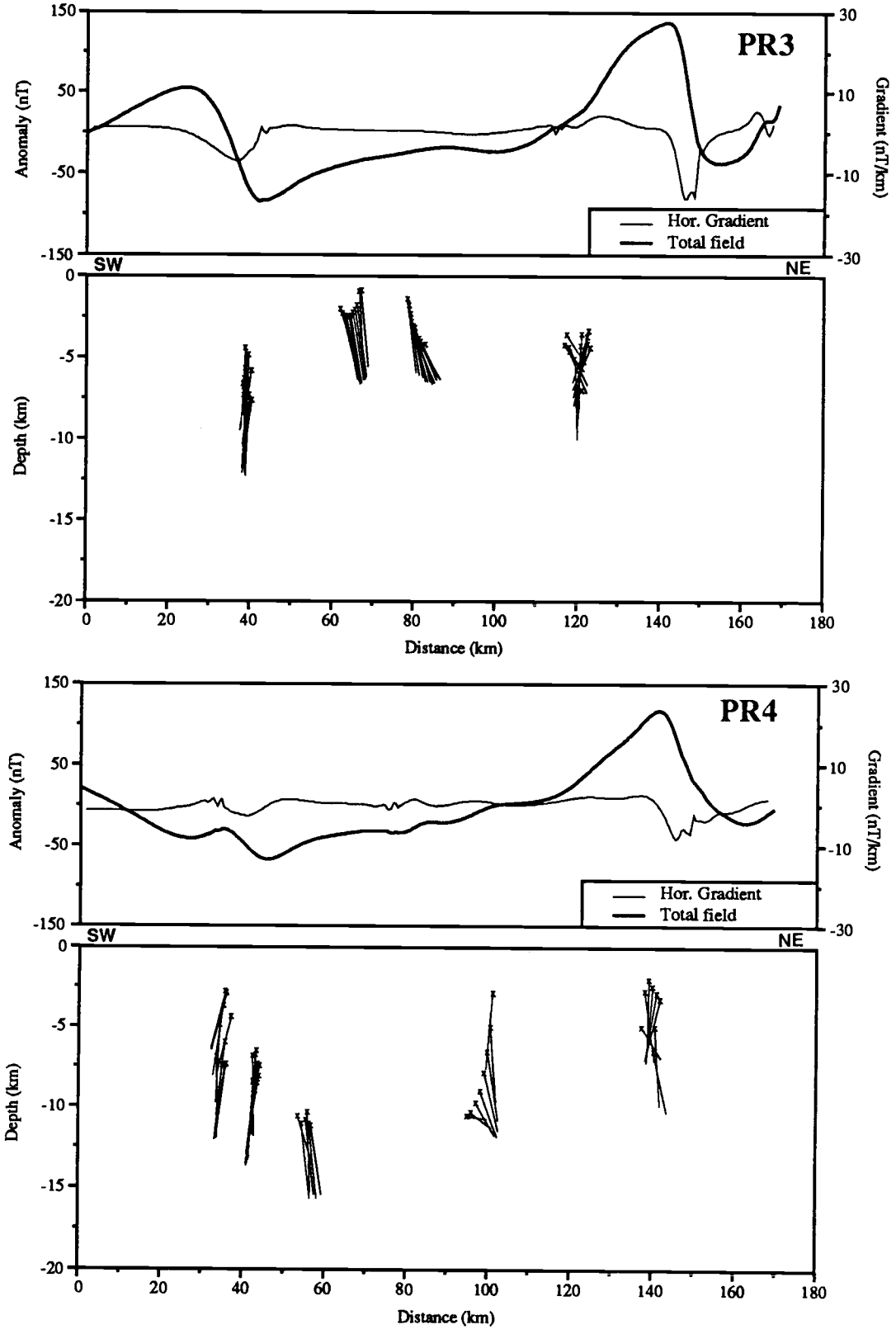

Figure 12. Magnetic anomalies and Werner solutions of profiles PR3 and PR4.

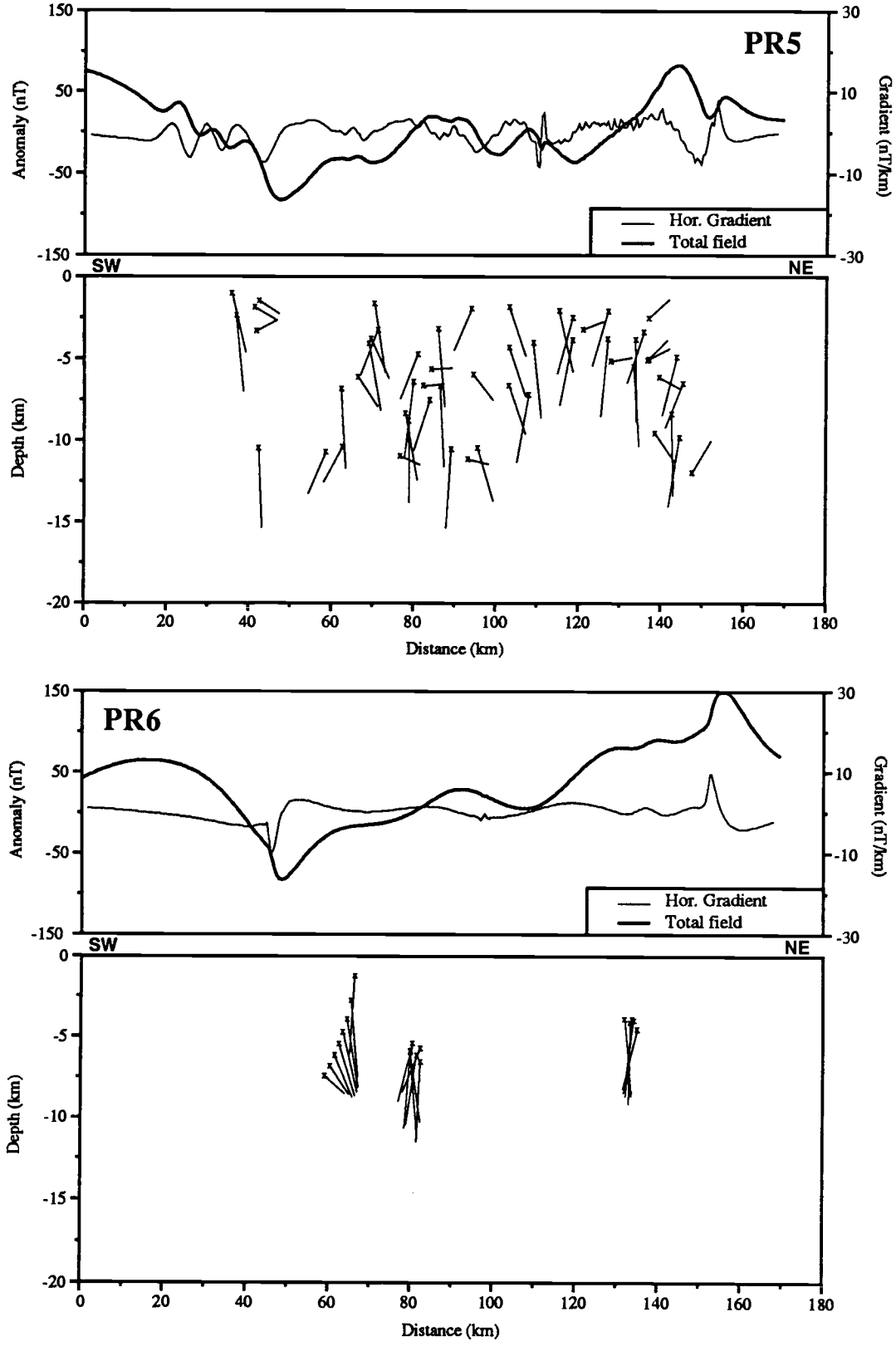

Figure 13. Magnetic anomalies and Werner solutions of profiles PR5 and PR6.

Profile PR1 shows 2 clusters of solutions well grouped at a shallow depth. Although it crosses the main magnetic anomaly of the northern Gulf, where it has its highest value, of about 150 nT, no obvious solution can be found regarding the presence of an interface. This is due to the broadness of the anomaly in this area. On all the other profiles, and at the left edge of PR1, the assumption of an average anomaly size of 30 km is valid; this does not hold true for the eastern part of the profile, where the width of the anomaly is in the order of 60 km. Using a Werner operator of .8 (as displayed in Figure 10) and a 30 km estimated anomaly size, requires a moving window of 24 km — less than twice the real width of the anomaly. A run with the new anomaly size of 60 km reveals the presence of an interface, although the first two solutions, while still present, are not as well defined.

Profile PR2 (Figure 10) shows 3 solutions. Only the third one contains a sufficient number of estimates to be well defined. The first two are consistent only in horizontal location and vary greatly in depth. They have to be considered as indicators only, not as definite solutions. Note the roughness of the real anomaly curve, compared to the synthetic models used in the previous chapter. This may be one of the reasons why so few solutions result from this run. The leftmost solutions (around km 40) seem to correspond to a well defined anomaly.

Profile PR3 is an example where 4 solutions are well defined. Although the magnetic profile itself is very smooth, giving way to an even smoother horizontal gradient with no visible characteristics, the computed solutions are well grouped. The first cluster yields a good consistency with respect to the dip angle, which is normal at this location. The next two clusters are much shallower (around 2 to 3 km), while the last cluster features good depth and location grouping, but a dip angle that varies widely.

On profiles PR3, PR4, PR5 and PR6, I have to take into account that the western edge of each profile is affected by the cosine taper that was applied to the grid from which these profiles were extracted. Therefore, solutions are generated which are not true solutions. With this in mind, the first solution of PR3 and PR4 might be dismissed as being generated by the taper. No land data was used to generate this grid.

Profile PR5 yields no solutions, yet all of the inconclusive estimates are shown in order to demonstrate what happens when the moving window (24 km) is larger than the average anomaly (15-20 km). The window straddles the top of different anomalies and is therefore unable to give a correct estimate. Reducing the anomaly size or the operator corrects this problem, but the number of estimates obtained thereafter in each cluster is still too small to make a statistically sound decision as to the validity of a solution.

Profile PR6 shows 3 solutions, though the first one is widely spread in depth from 2 to 7 km. The other 2 solutions feature good clusters, although they include only a few estimations each. The third solution, in particular, is shown here only as an indicator.

The result of these computations can be summarized by drawing a fault map containing all the solutions given by the Werner deconvolution (Figure 14). Fault locations on this map, obtained solely from the magnetics data, may be compared to the faults and lineaments shown on the tectonic map of Ness and Lyle (1988) . All of the principal faults found by my analysis occur at about the same location as those shown by Ness and Lyle. This is particularly true for the Tiburon and Consag Faults, while the Wagner Fault appears to be located more easterly and extends farther south. The South Cerro Prieto Fault agrees quite well in the north, and then takes on a more southerly trend. The Salsipuedes Fault does not appear in any of these computations since it is too close to the edge of the survey to allow for this kind of analysis.

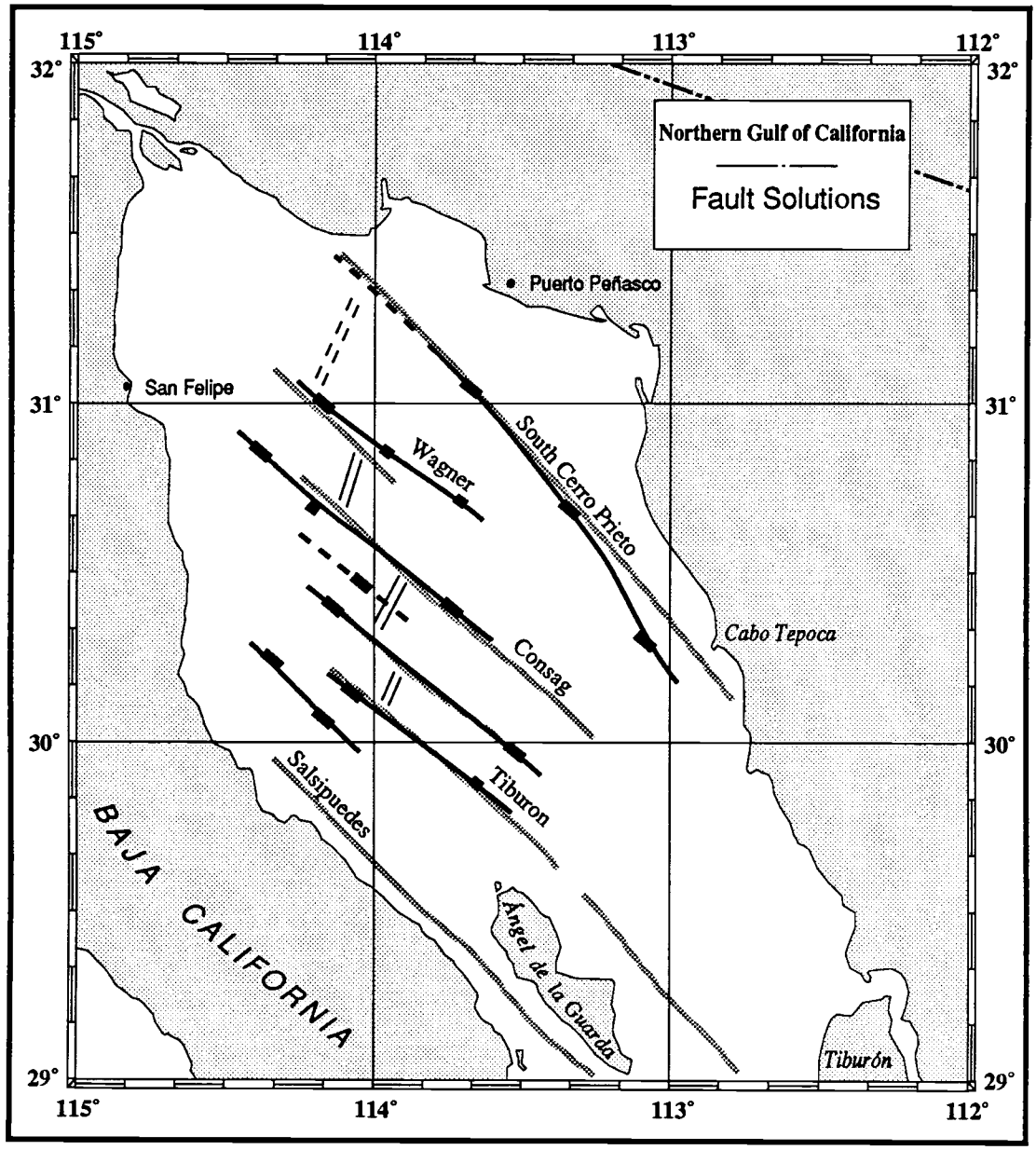

Figure 14. Tectonic map of the Northern Gulf of California using the Werner deconvolution method.

Depth to the Tops of the Faults

Another result that can be obtained from the deconvolution of magnetic profiles is the depth at which events occur. Kilty (1983) points out that among the parameters computed through this method, the horizontal location and depth of the dike or interface are the most reliable while the dip angle and magnetic susceptibility are strongly affected by the choice of the interference function representing the regional and neighboring features. I have shown that the horizontal location can be displayed through a pattern of faults. Similarly, depth information given by the deconvolution can be used to assess the topography of the structural layer containing the magnetized features. Once again it is assumed that any solution given by the deconvolution applied to the horizontal gradient of the total field anomaly may be represented as a fault or interface between two blocks.

In order to gather this information with maximum resolution available, a new array of 17 profiles will be used to cover the northern Gulf. Although the grid containing the magnetic data has a sample spacing of about 1 km, the trackline separation from the combined 1981 and 1984 cruises was in the order of 10 km. The spacing between the new profiles was chosen to be 12 km to avoid over-sampling, and also to make the best possible use of the available magnetics data. The locations of these profiles are shown in Figure 15.

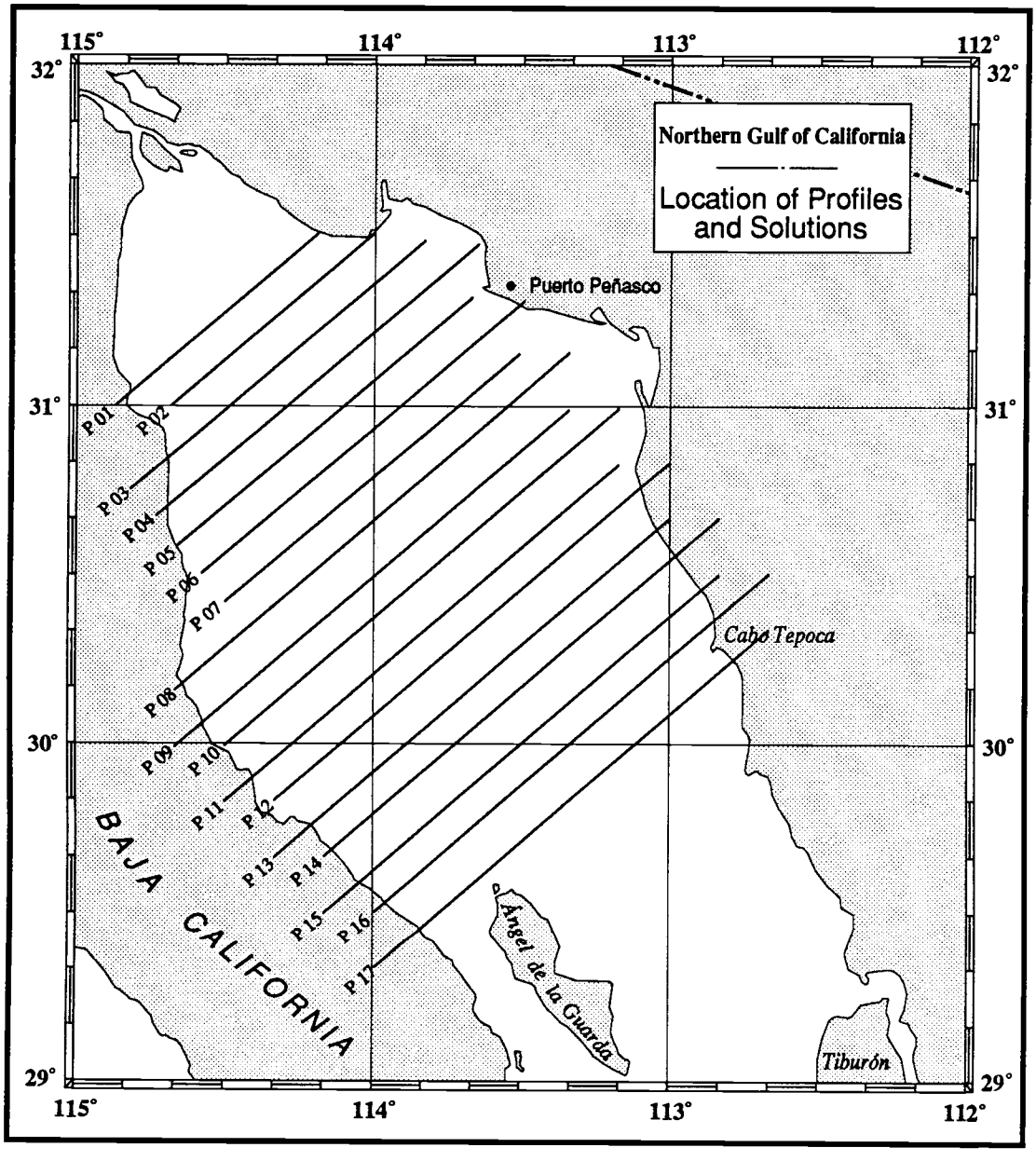

Figure 15. Location of magnetic profiles P01 to P17.

Appendix A contains the plots of profiles P01 through P17. Each plot displays the total field anomaly, the horizontal gradient of the total field and the solutions given by the Werner deconvolution in terms of horizontal location and depth of each estimated interface, after removal of stray solutions and statistical decision. As before, the average anomaly length was kept at 30 km except for profile P05. This was run with a average anomaly length of 20 km — the results being inconclusive when using 30 km. Note that this is equivalent to reducing the Werner operator by two-thirds, since the moving window is the product of these two parameters. Though profile P02 does show a cluster, the number of estimates for this cluster is too low provide a credible solution. Therefore, it is not included in the results for the array of the profile given in Table 3. Likewise, P13 does not present any credible solution, displaying instead a scatter of individual estimates with no apparent pattern. This is not surprising since profile P13 almost exactly crosses the same area as profile PR5, where this phenomena also occurred. The widely varying anomaly observed on top of this profile is perhaps due to crossing errors in the navigated tracklines, which the gridding process could not eliminate.

The clusters of solutions do not always appear at locations where they might be expected from the shape of the anomaly. Profiles P03, P04 and P05 do not display a fault pattern below the relative anomaly high to the east end of these profiles and profile P17 for example exhibits a cluster of solutions below its flattest

Profile	Location (km)	Depth (km)
P01	38	6
P03	34	5
	39	9
	58	8
P04	21	5
P05	34	3
	65	2
P06	36	10
	62	6
	98	5
P07	98	5
P08	16	4
	22/40	
	46	3
P09	40	7
	62	2
	84	4
	120	4
P10	22	12
	72	6
	118	4
P11	34	5
	43	8
	115	5
	140	5
P12	33	9
	46	4
	75	5
	100	3
	152	4
P14	35	10
	65	9
	140	6
P15	80	6
	134	4
P16	50	6
	72	2
	128	7
	136	2
P17	95	1

Table 3. Werner solutions for profiles P01 to P17.

section, where the anomaly decreases almost monotonically from -35 to -50 nT over a span of 40 km.

Figure 16 is a contour map of the depth to the tops of the faults obtained using the Werner deconvolution. The map is contoured at 2 km intervals. While no obvious lineations are present on the map, it does exhibit some distinct characteristics. The deepest area northwest of Angel de la Guarda island corresponds to the location of the Delfin Basin. Northwest of this area there exists another feature at a depth greater than 8 km. Another deep contour also agrees well with the location of the Consag basin, near 114°20'W and 30°40'N. The top of this structure is also more than 8 km deep.

The northeast section of the map is relatively flat, with depths to the top of the magnetic structures varying around 4 to 5 km. This generally agrees with the geophysical cross section shown in Figure 6, in which this range of depth describes the top of the magnetic basement.

The map also correlates well with the depth to intermediate magnetic sources found by Sanchez-Zamora (1988) from spectral analysis of magnetic data using a 2D-FFT method. Sanchez-Zamora proposed that the depth to the top of the shallow magnetic source present in his analysis represents the top of the structural basement. This is also in agreement with depths computed by Phillips (1964) from seismic refraction data. While no seismic refraction lines were shot in the western part of the northern Gulf where the main

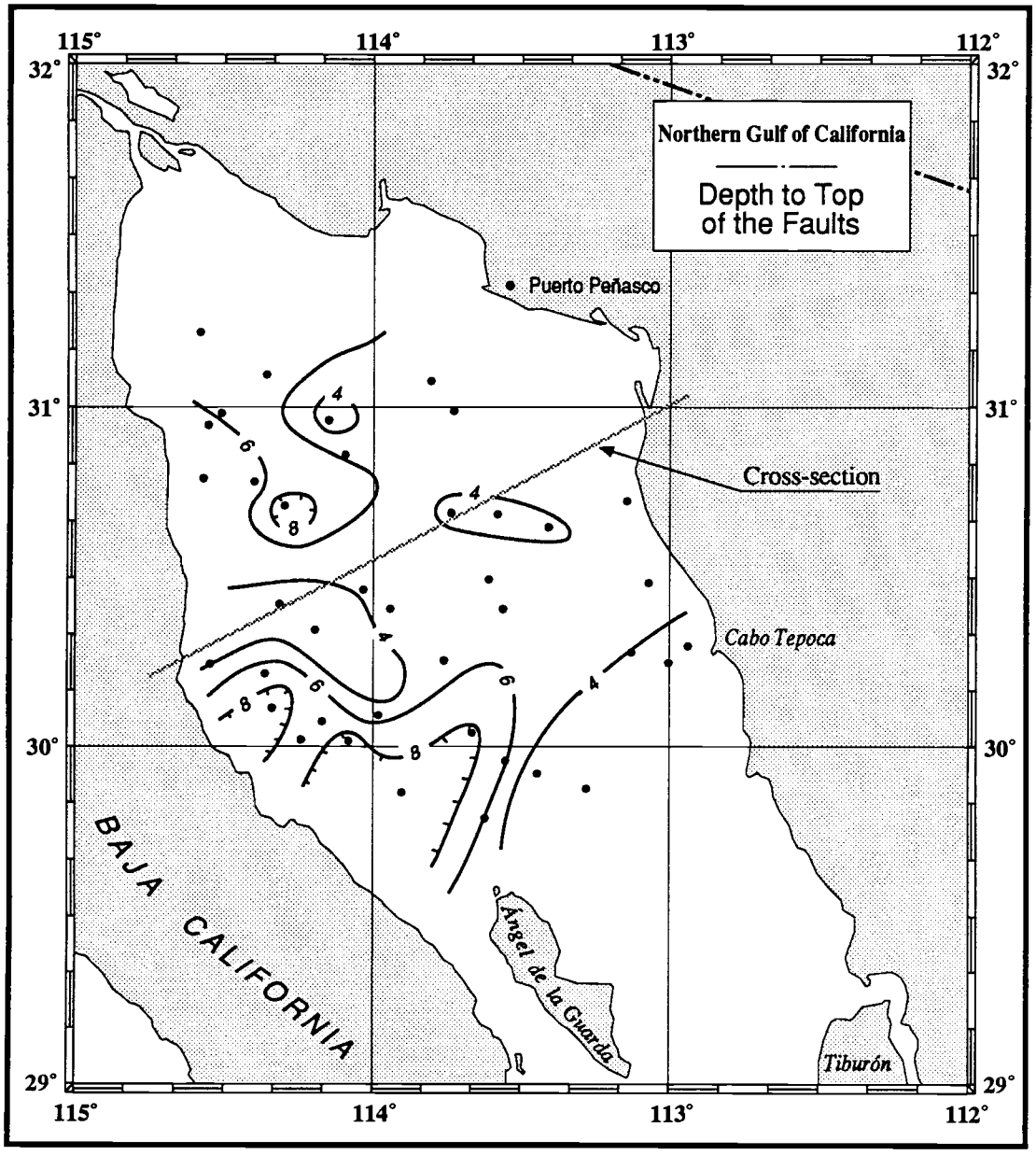

Figure 16. Contour map of the depth to the top of the faults.

features revealed by the Werner deconvolution method appear, the eastern and northern part of the map exhibit depths in good agreement with the findings of Phillips. Based on these agreements, I conclude that the depths obtained from the Werner deconvolution method represent the top of the structural basement in the eastern part of the Gulf while deeper estimates in the western part tend to suggest that the faulting that occurred around the Salsipuedes Fault zone took place in the lower basement, rather than in the upper basement.

CONCLUSIONS

This research was intended to add some detail to the present limited understanding of basement structure in the northern Gulf of California. I have accomplished this through geophysical modeling of a section across the Gulf and by applying an automated magnetic analysis method to resolve fault patterns.

The geophysical model constructed incorporates all available constraints: bathymetric, gravity, magnetics and seismic refraction, as well as magnetic horizons obtained from spectral analysis of magnetic data. This modeled section complements the sections of Plawman (1978) in the Imperial Valley and Calderon (1978) across the central Gulf. From the model, the crust is found to be about 18 km thick under the northern Gulf. An anomalous piece of high-density lower basement to the west of the section probably corresponds to the center of the divergence zone beneath the northern Gulf.

I have presented an implementation of a deconvolution method for the automated interpretation of magnetic profiles based on Werner's formulation of the thin-dike problem. I have extended the method using the fact that the horizontal gradient of the total field caused by the edge of a thick interface body is equivalent to the total field from a thin dike. Statistical decision making and a judicious choice of a Werner operator are necessary steps in obtaining a good

resolution for the computations of the horizontal location, depth, susceptibility contrast and dip angle. It should be possible to further refine the method so that this trial and error procedure could be eliminated, resulting in a truly automated process. The application of this technique to magnetic data from the northern Gulf of California proved successful with respect to locating fault zones (Figure 13) and the results are in good agreement with previously published literature. The depths to the top of the faults are interpreted as representing the top of the structural basement, though the deeper values computed for the western part of the Gulf may indicate that faulting does not occur in the upper basement in this area, but rather in the lower basement.

BIBLIOGRAPHY

Barday, R. J., 1974, Structure of the Panama basin from marine gravity data, M.S. Thesis, Oregon State University, 99 p.

Briggs, I. C., 1974, Machine Contouring Using Minimum Curvature, Geophysics, **39**, 39-48.

Calderón-Riveroll, G., 1978, A Marine Geophysical Study of Vizcaíno Bay and the Continental Margin of Western México Between 27° and 30° N Latitude, Ph.D. Thesis, Oregon State University. Corvallis, Oregon. 178 p.

Couch, R. W., O. Sánchez Z., P. Doguin, T. L. Plawman, G. Calderón R., S. P. Coperude, and B. Huehn, 1988, Geophysical Sections of the Gulf and Peninsular Province of the Californias, In: The Gulf and Peninsular Province of the Californias, J. P. Dauphin (ed), AAPG Memoir (in preparation), Tulsa.

Christensen, N. I., and M. H. Salisbury, 1975, Structure and constitution of lower oceanic crust, Rev. Geophys. Space Phys., **13**, 57-86.

Crowell, J.C., 1962, Displacement along the San-Andreas fault, Geol. Soc. America Spec. Paper 75, 61 p.

Elders, W. A., R. W. Rex, T. Meidav, P. T. Robinson and S. Biehler, 1972, Crustal spreading in Southern California, Science, **178**, 15-24.

Fuis, G. S., W. D. Mooney, J. H. Healy, G. A. McMechan, and W. J. Lutter, 1984, A seismic survey of the Imperial Valley Region, California, J. of Geophys. Res., **89**, 1165-1189.

Gerald, C. F., and Wheatley, P. O., 1984, Applied Numerical Analysis, Addison-Wesley Publishing Company, 191-193.

Goff, J. A., E. A. Bergman, and S. C. Solomon, 1987, Earthquake source mechanisms and transform fault tectonics in the Gulf of California, J. of Geophys. Res., **92**, 10485-10510.

Harrison, J. C., and S. P. Mathur, 1964, Gravity anomalies in Gulf of California, In: Marine Geology of Gulf of California, T.H. van Andel and George G. Shor (eds), Tulsa, AAPG Memoir, **3**, 122-125.

Hartman, R. R., Tesky, D. J. and Friedberg, J. L., 1971, A system for rapid digital aeromagnetic interpretation, Geophysics, **36**, 891-918.

Henyey, T. L., and J. L. Bischoff, 1973, Tectonic Elements of the Northern Part of the Gulf of California, GSA Bull., **84**, 315-330.

Hilde, T. W. C., 1964, Magnetic profiles across Gulf of California, In: Marine Geology of Gulf of California, T.H. van Andel and George G. Shor (eds), Tulsa, AAPG Memoir, **3**, 122-125.

International Association of Geomagnetism and Aeronomy, 1982, International Geomagnetic Reference Field 1980, Report, Geophysics, **47**, 841-842.

Jain, S., 1976, An automatic method of direct interpretation of magnetic models, Geophysics, **41**, 531.

Kasser, M., J.-C. Ruegg, P. Lesage, L. Ortlieb, J. Pagarete, N. Dutch, J. Guerrero, and J. Roldan, 1987, Geodetic measurements of plate motions across the central Gulf of California, Geophys. Res. Lett., **14**, 5-8.

Kilty, K. T., 1983, Werner deconvolution of profile potential data, Geophysics, **48**, 234-237.

Klitgord, K. D., J. D. Mudie, J. L. Bischoff, and T. L. Henyey, 1974, Magnetic Anomalies in the Northern and Central Gulf of California, GSA Bull., **85**, 815-820.

Ku, C. C., and Sharp, J. A., 1983, Werner deconvolution for automated interpretation and its refinement using Marquardt's inverse modeling, Geophysics, **48**, 754-774.

Larson, P. A., J. D. Mudie, and R. L. Larson, 1972, Magnetic Anomalies and Fracture-Zone Trends in the Gulf of California, GSA Bull., **83**, 3361-3368.

Lomnitz, C., F. Mooser, C. R. Allen, J. N. Brune, and W. Thatcher, 1970, Seismicity and Tectonics of the Northern Gulf of California Region, México, Geofísica Internacional, **10**, 37-48.

Ludwig, W. J., K. E. Nafe, and C. L. Drake, 1970, Seismic refraction, in: The Sea, v. 4, Part I, A. Maxwell (ed.), New-York, John Wiley and Sons, Inc., 53-84.

Menke, W. H., 1984, Geophysical Data Analysis: Discrete Inverse Theory, Academic Press, 209-218.

Moore, D. G., and E. C. Buffington, 1968, Transform Faulting and Growth of the Gulf of California Since the Late Pliocene, Science, **161**, 1238-1241.

Ness, G. E., and M. Lyle, 1988, Seismo-Tectonics of the Gulf and Peninsular Province of the Californias, In: The Gulf and Peninsular Province of the Californias, J. P. Dauphin (ed), AAPG Memoir (in preparation), Tulsa.

Phillips, R. P., 1964, Seismic Refraction Studies in Gulf of California, In: Marine Geology of Gulf of California, T.H. van Andel and George G. Shor (eds), Tulsa, AAPG Memoir, **3**, 408 p.

Plawman, T. L., 1978, Crustal Structure of the continental borderland and the adjacent portion of Baja California between latitudes 30°N and 33°N, M.S. Thesis, Oregon State University, 72 p.

Radhakrishna Murthy, I. V., 1985, The midpoint method: Magnetic interpretation of dikes and faults, Geophysics, **50**, 834-839.

Rusnak, G. A., R. L. Fisher, and F. P. Shepard, 1964, Bathymetry and Faults of the Gulf of California, In: Marine Geology of Gulf of California, T.H. van Andel and George G. Shor (eds), Tulsa, AAPG Memoir, **3**, 59-75.

Sánchez-Zamora, O., 1988,Crustal Structure and Thermal Gradients of the Northern Gulf of California Determined Using Spectral Analysis of Magnetic Anomalies, PhD Thesis, Oregon State University, Corvallis, Oregon. 127 p.

Stanley, J. M., 1977, Simplified Magnetic Interpretation of the geologic Contact and Thin Dike, Geophysics, **42**, 1236-1240.

Sumner, J. R., 1972, Tectonic Significance of Gravity and Aeromagnetic Investigations at the Head of the Gulf of California, GSA Bull., **83**, 3103-3120.

Sykes, L. R., 1968, Seismological Evidence for Transform Faults, Sea-Floor Spreading, and Continental Drift, Princeton University Press, 120-150.

Sykes, L. R., 1970, Earthquake Swarms and Sea-Floor Spreading, J. Geophys. Res., **75**, 6598-6611.

Talwani, M., J. L. Worzel and M. Landisman, 1959, Rapid gravity computations for two-dimensional bodies with application to the Mendocino submarine fracture zone, Journal of Geophysical Research, **64**, 49-59.

Talwani, M., and Heirtzler, J. R., 1964, Computation of magnetic anomalies caused by two-dimensional structures of arbitrary

shape, in Computers in the mineral industries, G. A. Parks, Ed., Stanford University, 464-480.

Thatcher, W., and J. N. Brune, 1971, Seismic Study of an Oceanic Ridge Earthquake Swarm in the Gulf of California, Royal Astron. Soc. Geophys. Jour., **22**, 473-489.

Vine, F. J., 1966, Spreading of the Ocean Floor: New Evidence, Science, **154**, 1405-1415.

Werner, S., 1953, Interpretation of magnetic anomalies at sheet-like bodies, Sveriges Geol. Undersok., Ser. C., Arsbok. 43 (1949), no. 6.

Wilson, J. T., 1965, A New Class of Faults and their Bearing on Continental Drift, Nature, **207**, 343-347.

APPENDIX

Plots of Profiles P01 to P17

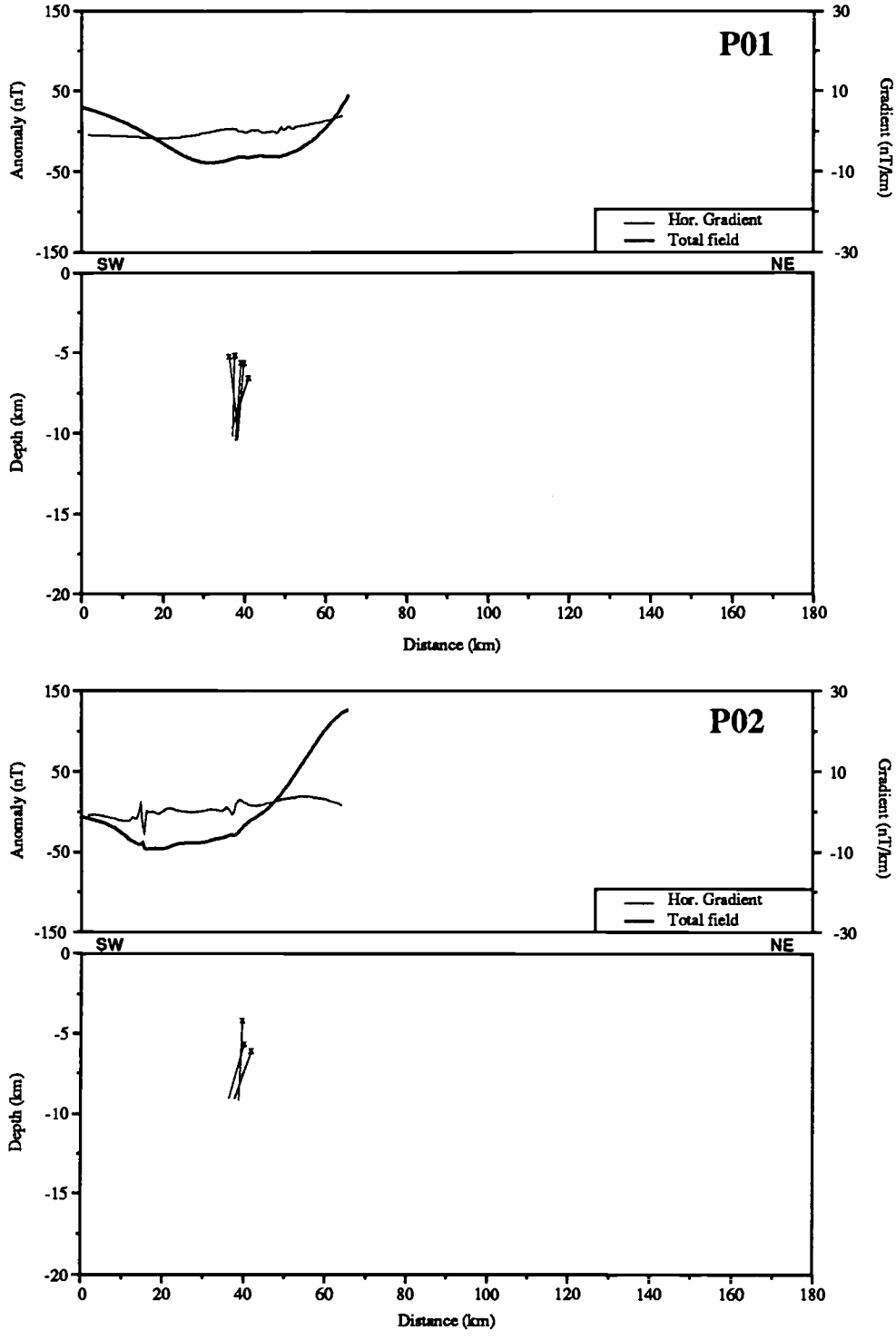

Figure A1. Magnetic anomalies and Werner solutions of profiles P01 and P02.

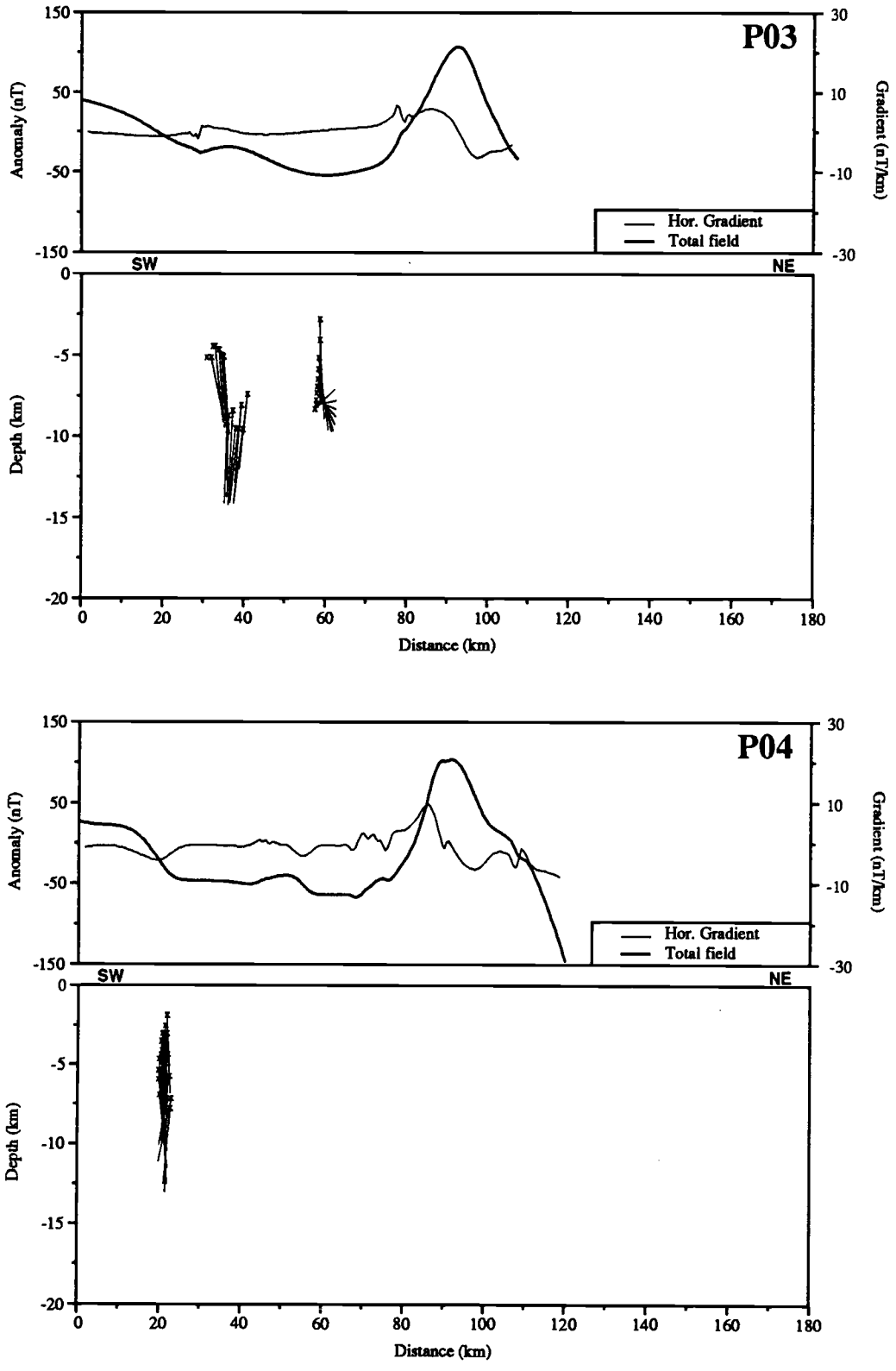

Figure A2. Magnetic anomalies and Werner solutions of profiles P03 and P04.

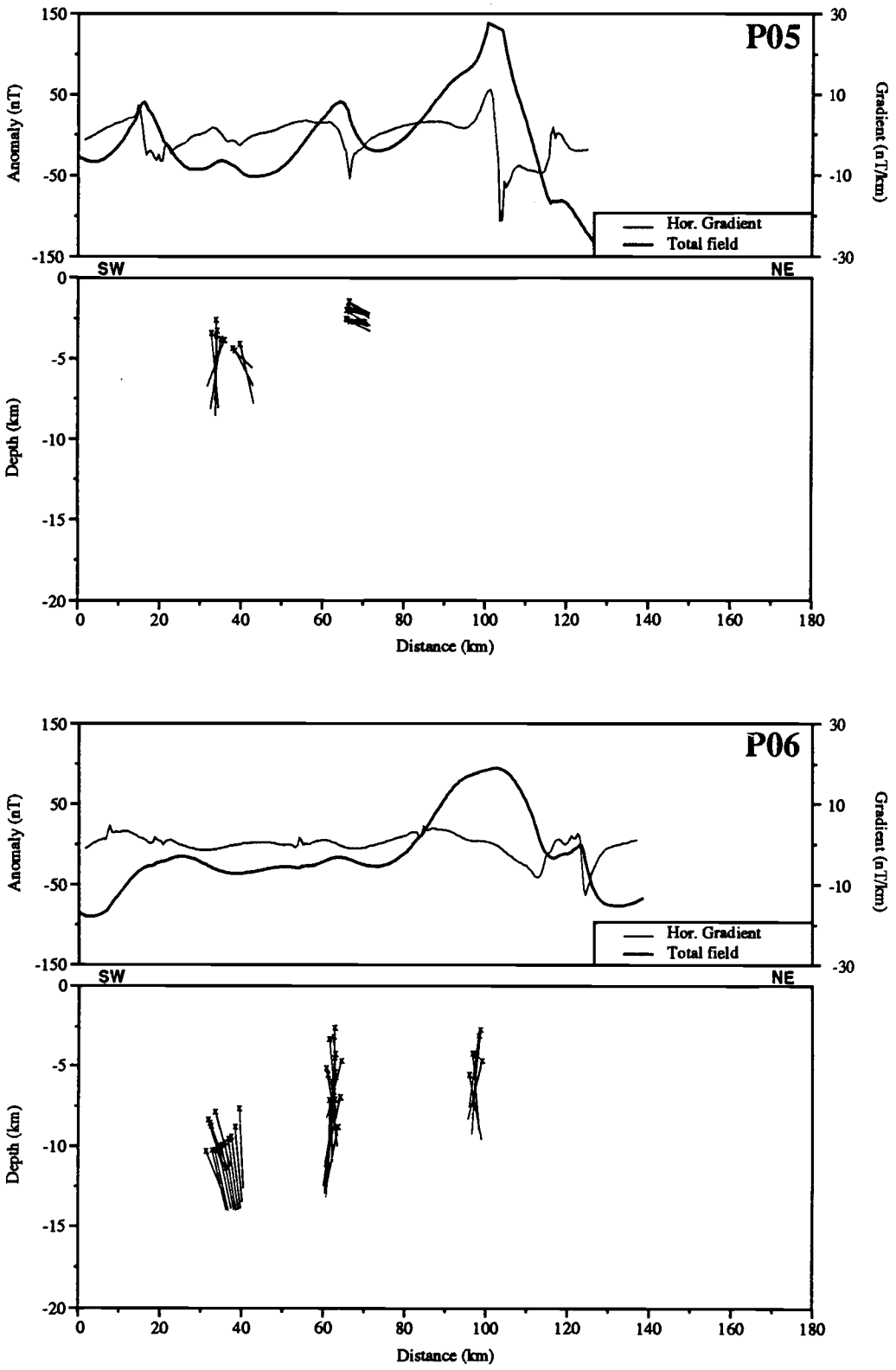

Figure A3. Magnetic anomalies and Werner solutions of profiles P05 and P06.

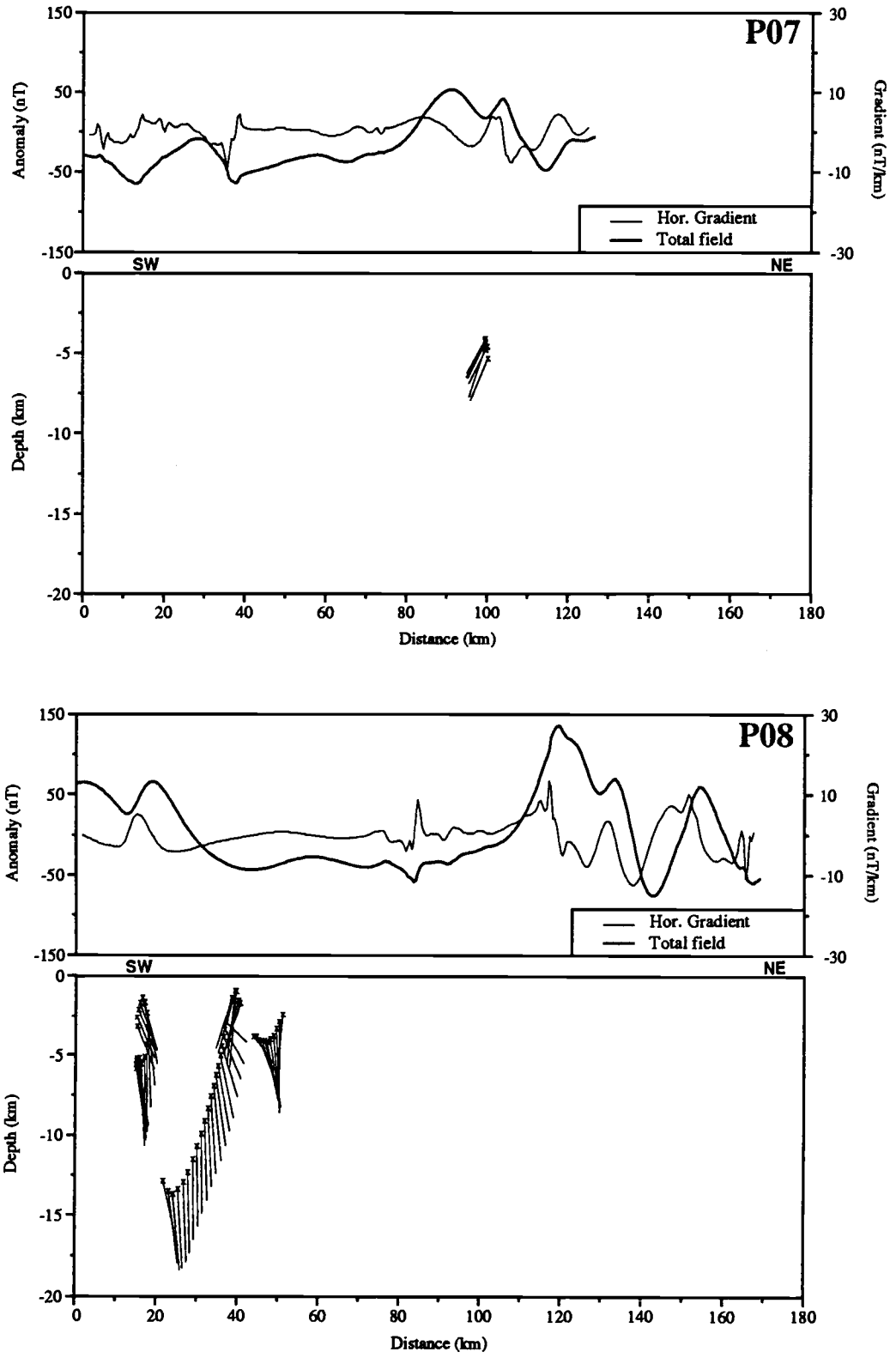

Figure A4. Magnetic anomalies and Werner solutions of profiles P07 and P08.

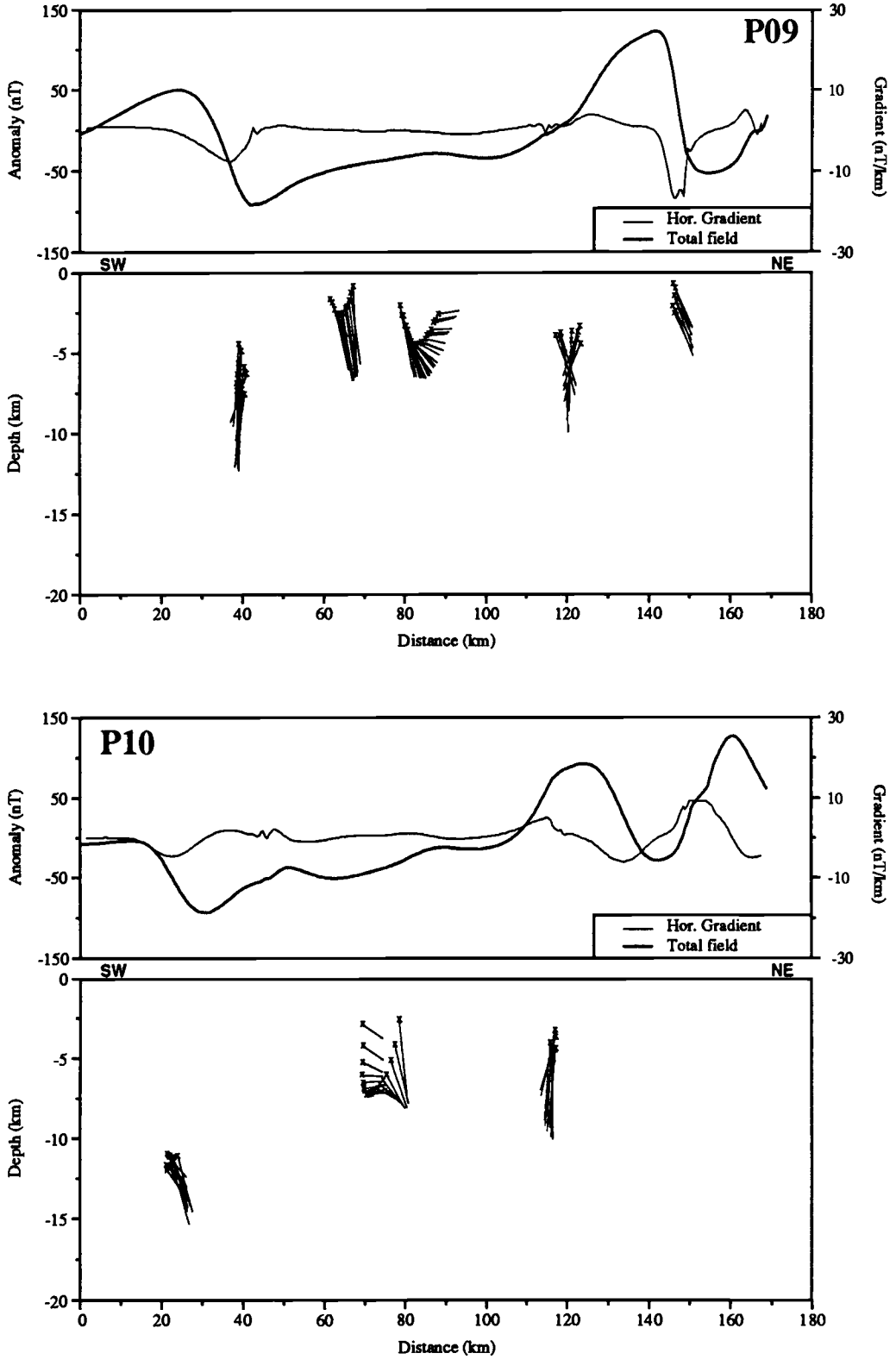

Figure A5. Magnetic anomalies and Werner solutions of profiles P09 and P10.

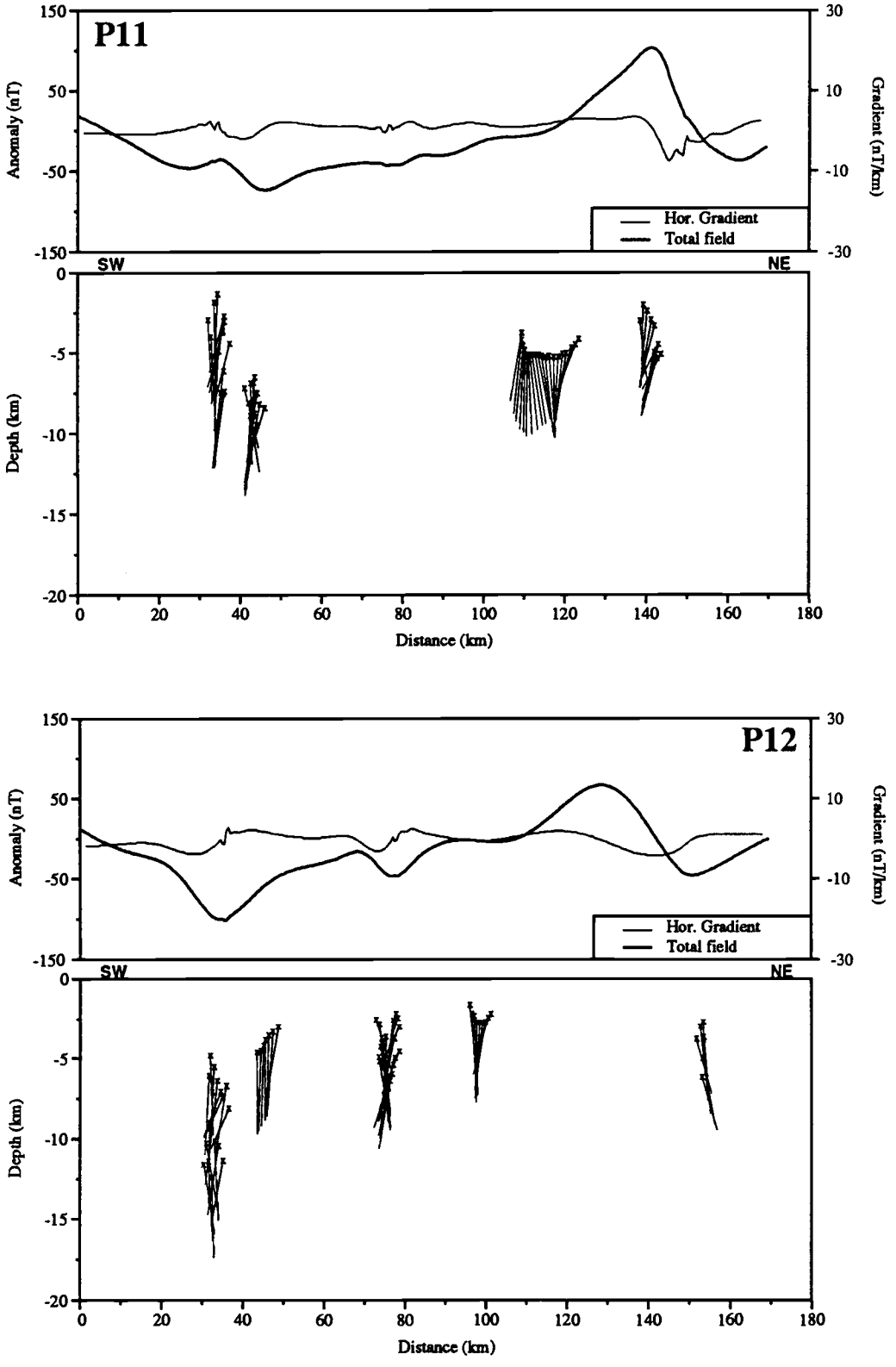

Figure A6. Magnetic anomalies and Werner solutions of profiles P11 and P12.

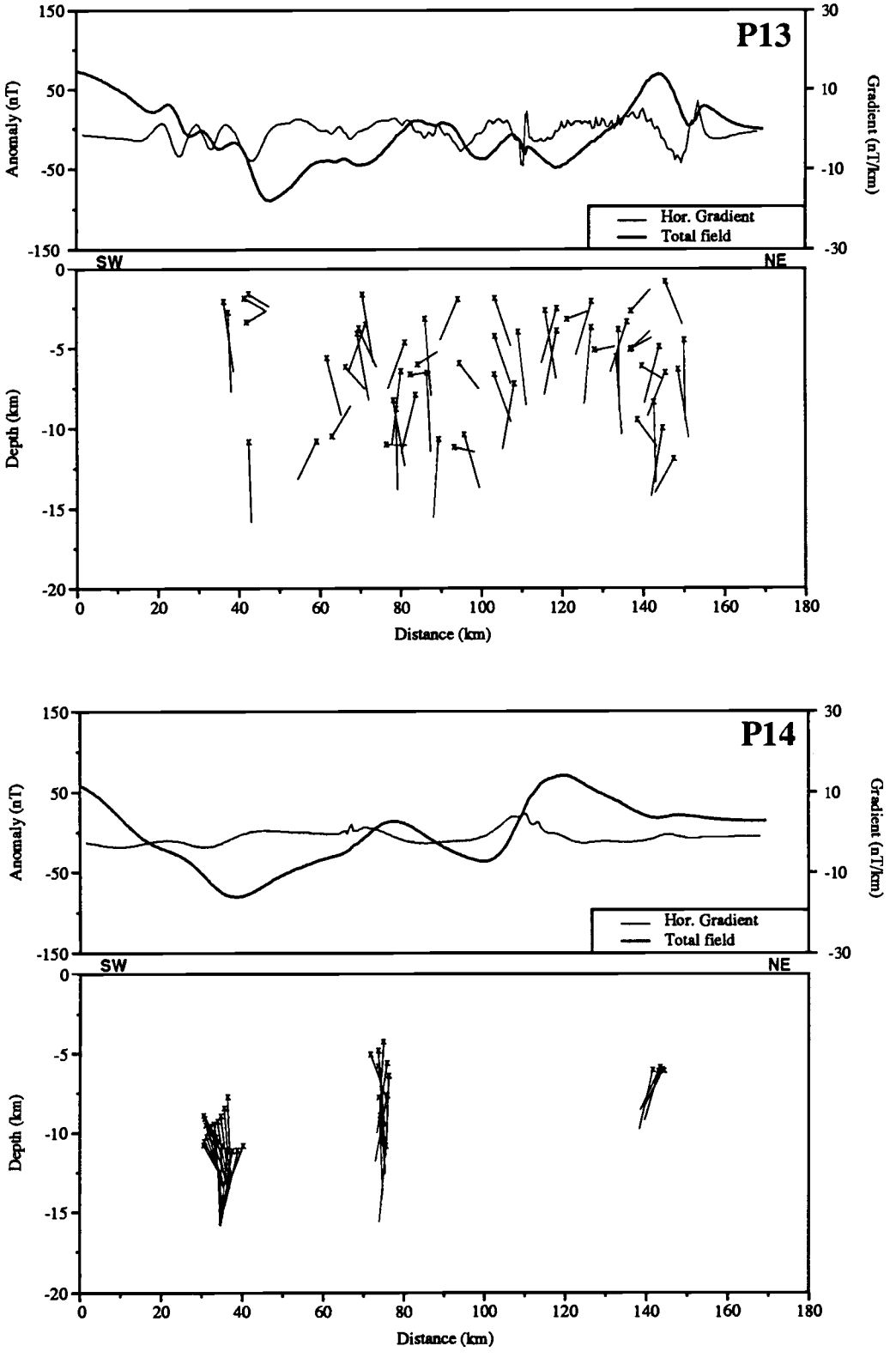

Figure A7. Magnetic anomalies and Werner solutions of profiles P13 and P14.

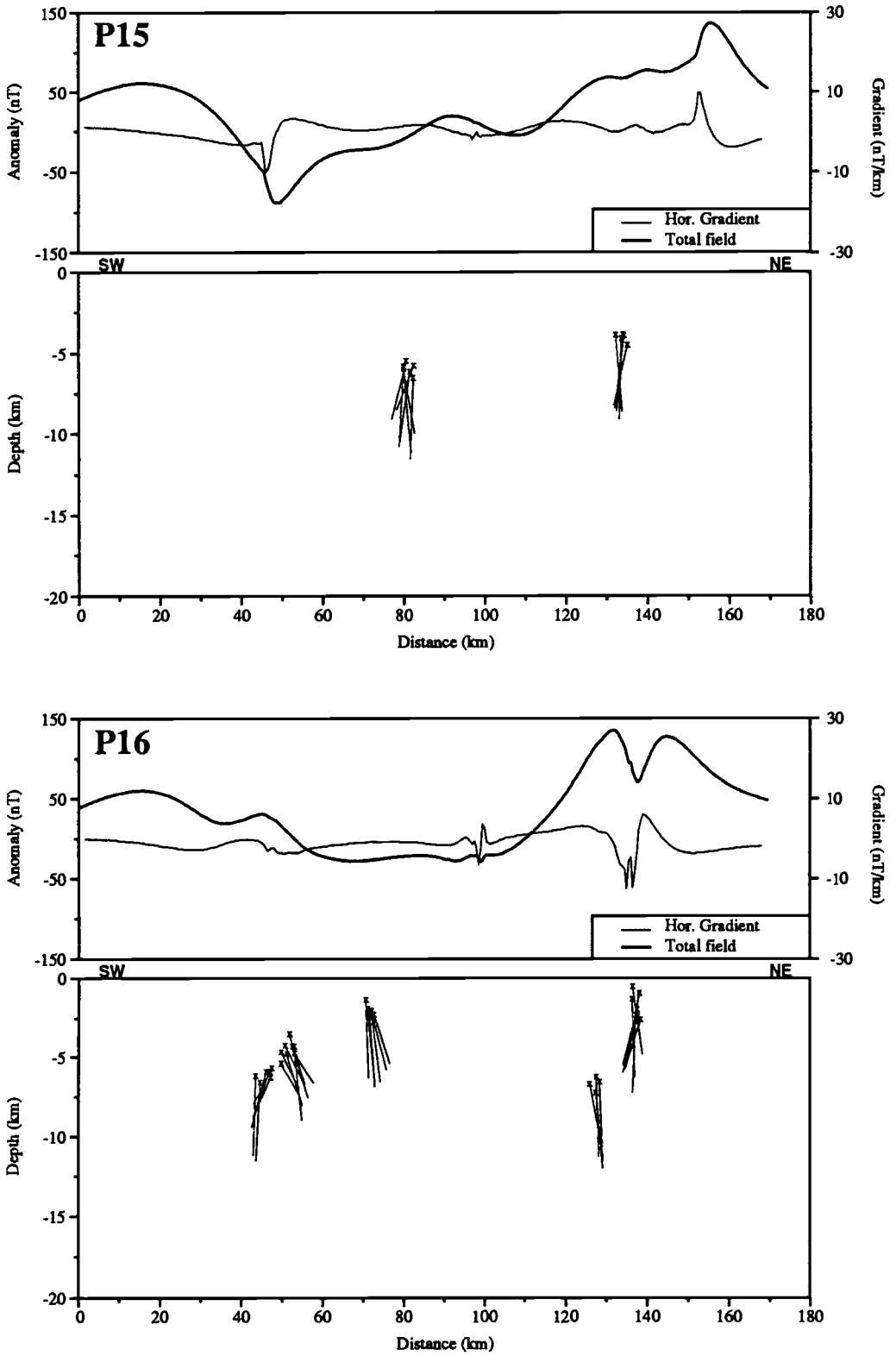

Figure A8. Magnetic anomalies and Werner solutions of profiles P15 and P16.

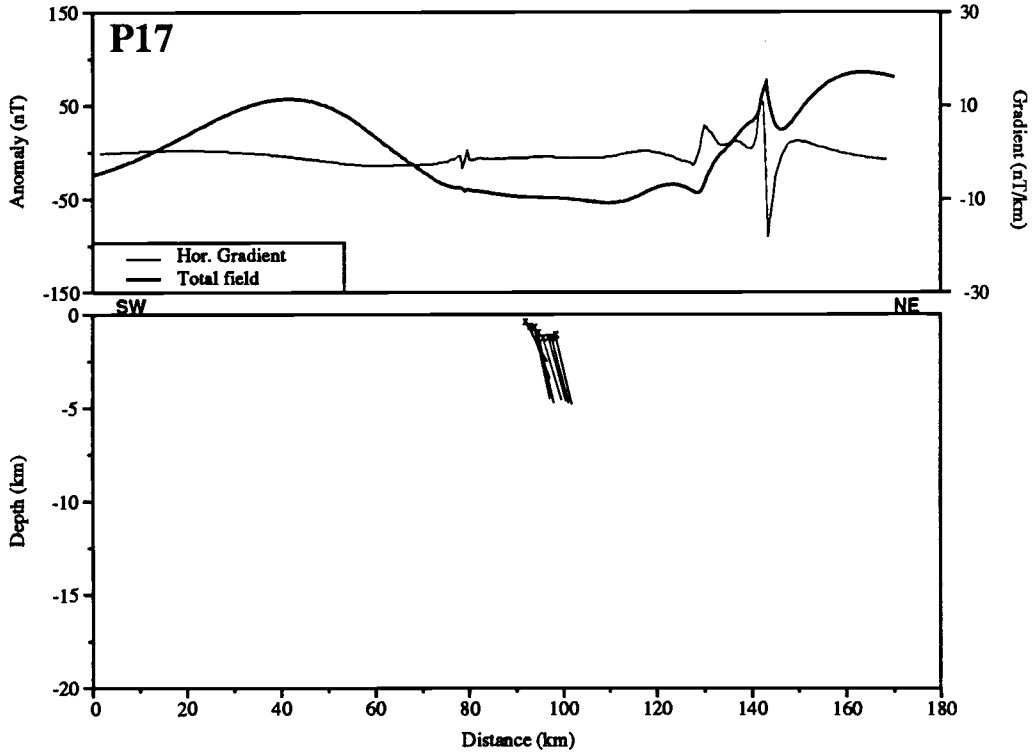

Figure A9. Magnetic anomalies and Werner solutions of profile P17.